Multi-scale phytoplankton dynamics in a coastal system of the Eastern English Channel: the Boulogne-sur-Mer coastal area

Kévin Robache[1,★], Zéline Hubert[1,★], Clémentine Gallot[1,2], Alexandre Epinoux[1], Arnaud P. Louchart[1,3], Jean-Valéry Facq[4], Alain Lefebvre[5], Michel Répécaud[6], Vincent Cornille[1], Florine Verhaeghe[1], Yann Audinet[1], Laurent Brutier[1], François G. Schmitt[1], and Luis Felipe Artigas[1]

[1]Université du Littoral Côte d'Opale, Université de Lille, CNRS, IRD, UMR 8187 LOG, Laboratoire d'Océanologie et Géosciences, F62930 Wimereux, France
[2]Mediterranean Institute of Oceanography (MIO), Campus de Luminy, 163 Av. de Luminy, f12288 Marseille cedex 9, France
[3]Netherlands Institute of Ecology (NIOO-KNAW), Department of Aquatic Ecology, Droevendaalsesteeg 10, 6708 PB Wageningen, The Netherlands
[4]Ifremer, Laboratoire d'Hydrodynamique Marine, F62200 Boulogne-sur-Mer, France
[5]Ifremer, COAST, Laboratoire Environnement et Ressources, F62200 Boulogne-sur-Mer, France
[6]Ifremer, Laboratoire Détection, Capteurs et Mesures, F29280 Plouzané, France
★These authors contributed equally to this work.

Correspondence: Kévin Robache (kevin.robache@univ-littoral.fr), Zéline Hubert (zeline.hubert@univ-littoral.fr), and Luis Felipe Artigas (felipe.artigas@univ-littoral.fr)

Abstract. To study changes in phytoplankton community composition at different time scales, an automated flow cytometer (Cytosub, Cytobuoy b.v.) was deployed on the MAREL Carnot automated monitoring station in Boulogne-sur-Mer (France) during spring (2021, 2022) and summer (2022), following an Eulerian approach. Phytoplankton dynamics were recorded every 2 hours, distinguishing 11 Phytoplankton Functional Groups (PFGs) based on optical and fluorescence properties. This enabled

5   detailed characterization of PFG successions, including MicroRED (mostly diatoms) and NanoRED (mostly haptophytes of the genus *Phaeocystis globosa*) transitions in spring, as well as a summer dominance by PicoORG (pico-cyanobacteria, mostly of the genus *Synechococcus*) and PicoRED. Four extreme events, including a salinity drop (April 2021), high winds (May 2021 and April 2022), and a marine heatwave (July 2022), caused rapid shifts in phytoplankton community composition. Empirical Mode Decomposition (EMD) and Lomb-Scargle Periodogram (LSP) analyses revealed that 85 ± 10 % of variability

10   in phytoplankton abundance, red fluorescence (proxy of chlorophyll *a*), and Shannon diversity occurred at relatively short timescales (9 hours to 11 days) for time series of several months, highlighting the value of high frequency monitoring in capturing ecological dynamics under macrotidal conditions in the Eastern English Channel.

1 Introduction

Phytoplankton, comprising unicellular autotrophic organisms suspended in the water column, are key primary producers in

15   marine ecosystems, driving carbon fixation and supporting heterotrophic organisms (Falkowski et al., 2003; Pal and Choudhury, 2014). They play a central role in marine food webs including microbial food web (Legendre and Rassoulzadegan, 1995), biogeochemical cycles, and the carbon biological pump. Despite constituting less than 0.1 % of global biomass, phytoplankton

contribute to approximately half of the world's annual net primary production (Falkowski et al., 1998; Field et al., 1998; Bar-On et al., 2018; Bar-On and Milo, 2019).

20   Coastal zones, which cover 12 % of the Earth's surface and accommodate between 23 % and 50 % of the global population (Crossland et al., 2005), are highly dynamic environments with significant ecological and socio-economic importance. These regions support 90 % of global fishing activity and exhibit high primary production driven by nutrient enrichment (Crossland et al., 2005; Cloern et al., 2014). Monitoring phytoplankton in these zones provides valuable insights into ecosystem health, helps us to better understand local ecosystems and offers indirect socio-economic benefits (Holland et al., 2023; Louchart et al.,

25   2023). Coastal waters are characterized by high spatio-temporal variability influenced by natural and anthropogenic factors, making them ideal for high frequency studies, which can capture rapid phenomena occurring within hours (Dubelaar et al., 2004; Kbaier Ben Ismail et al., 2016) and elucidating the strong spatio-temporal variability linked to meso and sub-meso scales processes (Rantajärvi et al., 1998; Bonato et al., 2015). These studies are especially valuable for understanding processes like Harmful Algal Blooms (HABs; Serre-Fredj et al., 2021) and multi-scale phytoplankton dynamics in connection to multi-scale

30   changes in coastal waters state (Hynes et al., 2024).

Phytoplankton dynamics respond rapidly to environmental changes driven by abiotic factors (e.g., turbulence, nutrients, temperature, salinity) and biotic factors (e.g., competition, predation, parasitism Smith and Lancelot, 2004; Menge and Weitz, 2009; Wyatt, 2014; Chiswell et al., 2015). Understanding these responses requires monitoring approaches that capture temporal variability. Eulerian and Lagrangian frameworks are often employed, but interpreting time series data can be challenging due

35   to the interplay between spatial and temporal changes.

In this study, we deployed an automated submersible "pulse shape-recording" flow cytometer, associated with physico-chemical parameters, on a coastal monitoring station in the Eastern English Channel (EEC). This instrument performs optical single-cell measurements every 2 hours, capturing phytoplankton dynamics from picophytoplankton (1 μm) to microphytoplankton (800 μm width; Pomati et al., 2013; Fontana and Pomati, 2014; Olson et al., 2003; Dubelaar et al., 2004; Louchart

40   et al., 2020). High frequency cytometry measurements has previously revealed insights into growth rates, physiological responses to extreme events, and community variability (Sosik et al., 2010; Dugenne et al., 2014; Thyssen et al., 2014). By deploying the automated flow cytometry in an Eulerian framework in a highly dynamic system submitted to anthropogenic pressure, we aimed to track phytoplankton variability across multiple timescales, capturing both periodic (e.g., tidal cycles) and non-periodic (e.g., extreme events) changes in functional groups and community composition. This approach allowed us

45   to explore phytoplankton dynamics over hours to months, enhancing our understanding of EEC coastal ecosystem variability.

2   Materials and methods

2.1   MAREL Carnot station

The MAREL Carnot station is an automated measurement platform, part of the National Observation Service and integrated into the COAST-HF network (https://coast-hf.fr; last accessed: 12th December 2024) integrated to the French National Struc-

50   ture for Littoral and Coastal Observation IR ILICO infrastructure (https://www.ir-ilico.fr; last accessed: 12th December 2024)
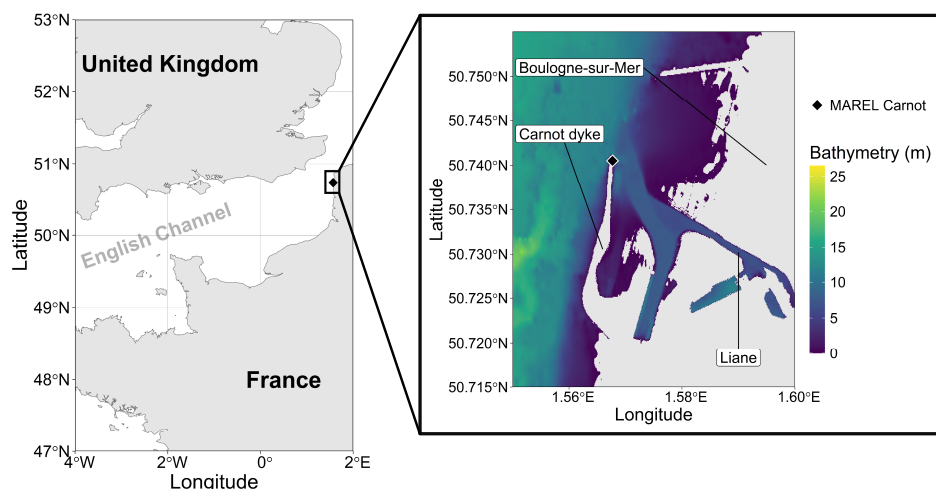
Figure 1. Map of the study area showing the location of the MAREL buoy on the Carnot dyke in Boulogne-sur-Mer. The bathymetry data, with an approximate resolution of 10 meters, were developed as part of the TANDEM project (SHOM, 2015). Only regions with bathymetric depths more than 0 m are displayed.

dedicated to high frequency monitoring of French coastal environments (Halawi Ghosn et al., 2023; MAREL Carnot, 2024). The station is situated at the end of the 2-km-long Carnot dike, near the lighthouse at the entrance of Boulogne-sur-Mer harbor (Pas-de-Calais, France), at the mouth of the Liane estuary (Fig. 1). This coastal area is subject to significant anthropogenic pressures, including those from harbor activities but also agricultural runoff entering the river (Lheureux et al., 2023). This

55 station continuously monitors subsurface (1.5 m depth) physico-chemical parameters at 20-minute intervals, including Sea Surface Temperature (SST), salinity, turbidity, dissolved oxygen, wind direction and speed, and fluorescence. A comprehensive description of these parameters is provided in Halawi Ghosn et al. (2023). As a fixed monitoring platform, it enables Eulerian observation of the marine environment by continuously recording temporal variations at a single location.

Wind data for 2021 were sourced from Météo France due to a lack of available data from the MAREL CARNOT sta-

60 tion during that period. Additionally, water height data for 2021 and 2022 were obtained from the 'Réseaux marégraphiques français' (REFMAR) data of the 'Service Hydrographique et Océanographique de la Marine' (SHOM, France). Furthermore, low-frequency nutrient data (ammonium, nitrite, nitrate, phosphate, and silicate) from the 'Suivi Régional des Nutriments' (SRN) program were utilized at the Boulogne 1 SRN-station off Boulogne-sur-Mer coastal area (the nearest low frequency monitoring station), as these parameters were not monitored by the station (Lefebvre et al., 2024).

65 The complex currents and the presence of multiple estuaries in the EEC (from the Somme estuary in Picardy, including the Liane estuary in Boulogne-sur-Mer, until the Slack estuary near the Strait of Dover, in addition to remote influence by the Seine estuary) contribute to the formation of the 'coastal flow' (Brylinski et al., 1991). This Region Of Freshwater Influence (ROFI) affects physico-chemical parameters, such as nutrients and salinity, which are influenced by freshwater discharge from

local or remote estuaries and land-based streams entering the sea. Along a coastal strip spanning 3 to 5 nautical miles, brackish
70 waters are observed, separated from the open sea by an interface similar to a desalination and tidal front (Brylinski et al., 1991).
These conditions significantly shape phytoplankton dynamics, particularly during recurrent seasonal events such as the spring
bloom, which is dominated in this region by an alternance of diatom and haptophyte (*Phaeocystis globosa*; Breton et al., 2000;
Lefebvre et al., 2011; Breton et al., 2022). The coastal waters off Boulogne-sur-Mer are characterized by a macrotidal regime
(tidal range > 4 m) and occasionally border on megatidal conditions (tidal range > 8 m; Levoy et al., 2000). The tides are semi-
75 diurnal, completing a full cycle approximately every 12.4 hours (Lazure and Desmare, 2012). During ebb tide, the current in
the EEC flows southwestward, while flood tide results in a northeastward flow, causing a reversal in currents during tidal shifts.
However, wind dynamics can significantly alter this circulation pattern, adding to the complexity of the hydrodynamics of the
EEC at various spatio-temporal scales (Lazure and Desmare, 2012; Bertin et al., 2024). The current patterns within the harbor
are also influenced by factors such as freshwater inflows and tidal phases, with an eddy typically forming during rising tide
80 (Jouanneau et al., 2013; Sentchev and Yaremchuk, 2016). Current speeds inside the harbor are generally lower than offshore
but remain substantial due to tidal influence, typically ranging between 0.1 m s^{-1} and 0.3 m s^{-1} (Sentchev and Yaremchuk,
2016). These speeds ensure that the water column remains well-mixed.

These hydrological characteristics play a crucial role in influencing phytoplankton dynamics across different timescales, as
plankton, by definition, is transported by currents.

2.2 Automated flow cytometer

A CytoSub (Cytobuoy b.v., Netherlands) was deployed in the MAREL Carnot station between March 23rd and May 12th 2021
then between March 17th and August 3rd 2022. This automated flow cytometer uses a 488 nm-laser (blue) to digitize the
optical features and pulse profile of particles. The interaction of each particle with the laser beam produces forward scatter
(FWS), which relates to particle size (Cunningham and Buonnacorsi, 1992), and side scatter (SWS), which provides informa-
90 tion about the internal and external complexity of the particles (Dubelaar et al., 2004; Fontana and Pomati, 2014; Fragoso et al.,
2019). It also measures three types of fluorescence (red, orange, yellow; FLR, FLO, FLY) corresponding to pigment compo-
sition: chlorophyll *a*, phycoerythrin and phycocyanin, and phaeopigments or degraded pigments, respectively (Dubelaar and
Gerritzen, 2000; Dubelaar and Jonker, 2000). The digitized profile yields different features such as the area under the curve,
maximum, and minimum, which are used to create 2-dimensional plots (cytograms). In these plots, particles are positioned
95 according to their optical properties, allowing for clustering (gating) of similar particles, as shown in Fig. 2.

Three cytometry protocols were used in this study, each optimized for specific size ranges. The "Pico" protocol targets
particles below 5 μm, while the "Micro" protocol captures particles above 5 μm. A third protocol, the "Micro-Photo", mirrors
the "Micro" protocol but uses a lower sample flow rate to acquire precise images of particles that compose the different nano-
and micro- Phytoplankton Functional Groups (PFGs; Thyssen et al., 2022). In 2021, a single threshold (or trigger level) based
100 on a minimum of FLR was applied for both protocols. In 2022, two detection thresholds were used during *in situ* measurements
by MAREL Carnot with the CytoSub, using both SWS and FLR signals to capture the longer pulse-shape. This adjustment
does not affect measures of PFGs abundance or total phytoplankton abundance. During this study, 11 PFGs were defined
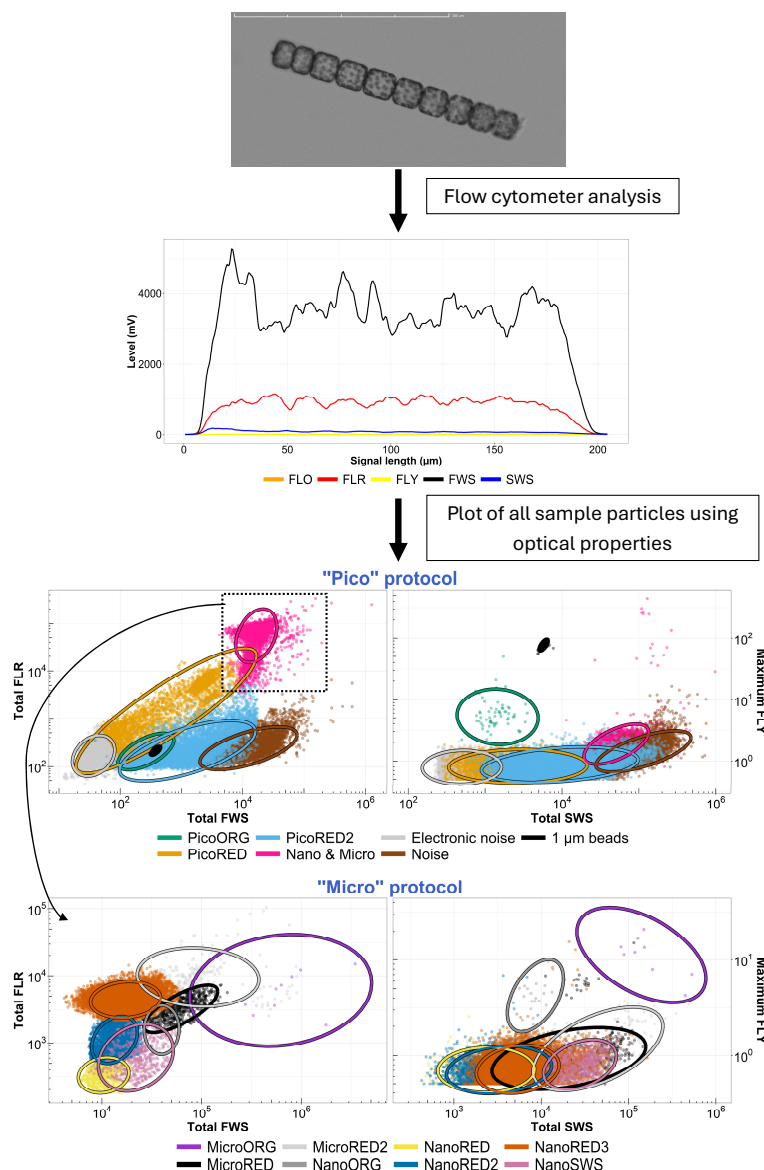
Figure 2. Diagram of the principle of the automated pulse shape-recording flow cytometer, from particles to cytograms. The top figure shows an example of picture of a colonial diatom (*Lauderia sp.*) taken by the CytoSub. Its associated optical spectrum is shown below. The cytograms shown at the bottom of the figure are based on the properties of the optical features of all the cells and colonies analyzed for a single sample, calculated from the optical signals recorded. The coloured scatter points and ellipses (t distribution confidence interval of 95 %) are shown as a gating example for these particles.

through manual clustering using CytoClus 4 software. The bibliographic context of the study area (Guiselin, 2010; Bonato et al., 2015; Louchart et al., 2020, 2024) and the "Micro-Photos" protocol enabled to interpret PFGs in term of probable

Table 1. Detailed glossary of characterized PFGs. The taxonomical/optical interpretation of each group is based on determination by images and literature. A particle belonging to a given group therefore has optical properties similar to those of the proposed optical equivalent even though it is uncertain that the observed particle corresponded to the given taxa (or attributed taxa). Thyssen et al. (2022) optical group common vocabulary equivalents are also provided.

Optical group	Example of taxonomical correspondence	Difference from similarly named groups	Standardised vocabulary
PicoRED	Autotrophic picoeukaryotes	Lower FWS	RedPico
PicoRED2	Autotrophic picoeukaryotes	Higher FWS	RedPico
PicoORG	Pico-cyanobacteria (mainly *Synechococcus* spp.)	-	OraPicoProk
NanoRED	Eukaryotic nano autotroph (mainly *P. globosa*, flagellated cells)	Lower FLR	RedNano
NanoRED2	Eukaryotic nano autotroph (mainly *P. globosa*, flagellated cells)	Medium FLR	RedNano
NanoRED3	Eukaryotic nano autotroph (mainly *P. globosa*, free colonial cells)	Higher FLR	RedNano
NanoORG	Eukaryotic nano autotrophs with phycoerythrin (mainly *Cryptophyceae sp.*)	-	OraNano
NanoSWS	High side-ward scatter eukaryotic nano autotrophs (mainly *Coccosphaerales sp.*)	-	HsNano
MicroRED	Eukaryotic micro autotrophs (mainly *Pseudo-Nitzschia* complex)	Lower FLR	RedMicro
MicroRED2	Eukaryotic micro autotrophs (mainly free and colonial diatoms)	Higher FLR	RedMicro
MicroORG	Eukaryotic micro autotrophs with phycoerythrin (mainly *Cryptophyceae sp.*)	-	OraMicro

105   taxonomic equivalents, which where additionally related to the novel consensual nomenclature published in Thyssen et al. (2022), as detailed in Table 1.

To facilitate comparisons between the two study years, Julian days (J_d) were standardized to the UTC +01:00 time zone (see Sect. 3.1).

2.3 Statistical analysis

2.3.1 Emirical Mode Decomposition and Lomb-Scargle Periodogram analysis (EMD-LSP)

The Empirical Mode Decomposition (EMD) was used to charaterize the multi-scale phytoplankton dynamics. This algorithm decomposes a time series $X(t)$ into n Intrinsic Mode Functions (IMFs) $C_i(t)$ as described by Huang et al. (1998):

$$X(t) = \sum_{i=1}^{n} C_i(t) + r_n(t) \tag{1}$$

EMD works by first constructing upper and lower envelopes that connect the local maxima and minima of the time series, respectively. The mean of these envelopes defines the first zero-mean IMF $C_1(t)$. This IMF is then subtracted from the original time series, and the process is repeated n times until a monotonic function $r_n(t)$, representing the trend of the series, is obtained (Huang et al., 1998). This decomposition method allows a time series to be expressed as a sum of oscillating modes, each with a distinct characteristic scale, alongside a trend. EMD has been previously used, for instance, to used to analyze phytoplankton dynamics in Lake Geneva (France-Swiss border) by Schmitt et al. (2013), where it was applied to study multi-scale variability.

To determine the mean period of each IMF, we applied the Lomb-Scargle Periodogram (LSP), a technique originally developed for analyzing irregular astronomical time series (Lomb, 1976; Scargle, 1982) but applicable to biological time series (Ruf, 1999). The LSP evaluates various periodic patterns by fitting sine or cosine waves of different frequencies, amplitudes, and phases to the observed data. The most appropriate pattern, including its phase and amplitude, is identified by determining the frequency of the sinusoidal waveform that best describes the observed data. Only frequencies above $2f_{min}$ were retained based on the Nyquist-Shannon theorem. The mean period $\overline{T_i}$ for each IMF was calculated using:

$$\overline{T_i} = \left(\frac{\int_0^\infty f L^s{}_i(f)\mathrm{d}f}{\int_0^\infty L^s{}_i(f)\mathrm{d}f} \right)^{-1}, \tag{2}$$

where f is the frequency and $L^s{}_i$ is the Lomb-Scargle spectrum of $C_i(t)$. This method provides an energy-weighted calculation of the mean period (Huang et al., 1998, 2009). Additionally, the period of the maximum peak in the periodogram, $T_{\max}$, was extracted.

To assess the contribution of each IMF to the total signal, we calculated their relative variance $V_i = V(C_i)$. The variance lost V_i^{lost} after removing the IMFs C_1 to C_i from the original signal was estimated using:

$$V_i^{\text{lost}} = 100 \cdot \frac{\sum_{k=1}^{i} V_k}{\sum_{k=1}^{n} V_k + V(r_n)}, \tag{3}$$

where n is the total number of IMFs found for $X(t)$. This calculation provides an estimate of the information loss across different timescales based on the periods of the different IMFs.

2.3.2 Shannon diversity index H'

We applied the EMD-LSP method to the exponential value of the Shannon diversity index H' (Shannon, 1948) based on the cytometric optical communities:

$$H' = -\sum_{i=1}^{S} p_i \log_2(p_i), \tag{4}$$

where $\log_2$ is the binary logarithm, S is the number of communities and p_i is the proportion of the community i in the entire ecosystem. The Shannon diversity index is widely used to characterize community diversity by considering both the richness (number of functional groups) and their relative abundances in a sample. It serves as an indicator of ecosystem health and can signal disturbance (Hill, 1973; Li, 1997, 2002). We examined the dynamics of its exponential form, known as Hill's diversity number of order one (Hill, 1973). This cytometric diversity index provides information about the non-taxonomic entropy of community assemblages and reflects the level of organization (in thermodynamic terms) of the ecosystem. The Shannon index dynamics capture how quickly the functional structure of a part of the ecosystem can change, as cytometric groups can be considered functional groups based on optical features as proxys of size, granulosity and pigment content (Le Quéré et al., 2005; Fontana and Pomati, 2014; Fragoso et al., 2019; Fuchs et al., 2022; Louchart et al., 2024).

Shannon entropy is fundamental in phytoplankton ecology as it determines the community structure and thereby can be linked to the environmental conditions. It has been previously applied to functional groups in other studies (e.g., Sun and Wang, 2021). Here, we applied the EMD-LSP analysis to the time series of $\exp(H')$ to explore the variability in the arrangement of communities over multiple timescales. The aim was to account for its multi-scale dynamics, spanning from hours to days, and to understand the dynamic shifts in community composition.

3 Results

3.1 Phytoplankton phenologies

The abundance and FLR data (both total and per optically-defined PFG) are shown in absolute values in Fig. 3 and in relative values in Fig. 4.

The dynamics of the 2021 spring bloom on a seasonal scale can be divided into three distinct phases. At the start of the measurement series ($J_d = 82$), the PicoRED2 group dominated, increasing from 8 % to 63 % of the total abundance between March 24th and March 26th ($J_d = 83$ and $J_d = 85$). During this period ($J_d \in [82; 96]$), total abundance ranged from $0.12 \cdot 10^4$ to $4.1 \cdot 10^4$ cells mL^{-1} (Fig. 3a). The second phase began on April 7th ($J_d = 97$), marked by the predominance of the NanoREDs groups. These groups, initially dominant at the start of the study period, became the majority again, with a mean contribution of 58.5 ± 11.3 % for $J_d \in [97; 121]$. Total abundance during this phase ranged from $0.47 \cdot 10^4$ to $11.87 \cdot 10^4$ cells mL^{-1} (Fig. 3a). This phase corresponded to the onset of the *P. globosa* bloom, a phenomenon typical of the EEC (Breton et al., 2022) and frequently monitored due to its classification as a HAB (Lefebvre and Dezécache, 2020). Notably, the contribution of this group to total phytoplankton abundance fluctuated, with periods of high relative abundance coinciding with local maxima

in total abundance, followed by brief declines. Hourly fluctuations were also observed, driven by extreme events in early May, which will be discussed in Sect. 3.2. Towards the end of the time series, the contribution of the NanoRED2 group to total abundance increased (12.8 % above the average for its associated PFG time series), while that of the NanoRED3 group decreased (5.9 % below its average).

170   In terms of FLR (a proxy for chlorophyll a biomass), a clear seasonal dynamic was observed. The MicroRED2 group was well-represented at the start of the bloom, spanning from approximately March 23rd to March 27th($J_d = 82$ to $J_d = 86$). Its contribution gradually declined through the beginning of April. As the season progressed, the NanoRED2 and NanoRED3 groups dominated the FLR time series, with rapid alternations in their relative importance. The peak in FLR was recorded on April 24th ($J_d = 114$), coinciding with the core of the NanoREDs bloom. This period, traditionally dominated by *P. globosa*, saw significant representation of the NanoRED2 and NanoRED3 groups.Towards the end of the bloom, starting on May 7th ($J_d = 127$) , the NanoRED2 group became increasingly prominent in contributing to total fluorescence. This pattern aligns with abundance data, where NanoRED2 accounted for 28.8 ± 6.0 % of cumulative total abundance, peaking at 51.4 % on May 8th.

The dynamics of the 2022 spring bloom can be divided into several phases. The first phase was dominated by the PicoREDs groups, which accounted for 83.4 ± 7.7 % of the total abundance during $J_d \in [76; 100[$, with a peak of $12 \cdot 10^4$ cells mL^{-1} recorded on April 9th ($J_d = 99$). The PicoORG group also contributed an average of 7 % between March 23rd and March 27th ($J_d = 82$ and 86). From April 10th ($J_d = 100$), an increase in the NanoREDs groups' total and relative abundances likely marked the onset of the *P. globosa* bloom. Between May 5th and May 27th ($J_d = 125$ to $J_d = 147$), their relative abundance averaged 45.8 ± 10.0 %, with absolute values ranging from $0.6 \cdot 10^4$ to $8.0 \cdot 10^4$ cells mL^{-1}. A succession was observed: NanoRED3 dominated between May 6th and May 16th ($J_d = 126$ to $J_d = 136$), followed by NanoRED2 from May 17th to May 26th ($J_d = 137$ to $J_d = 146$). Finally, from June 10th ($J_d = 161$), blooms of PicoRED, PicoORG (*Synechococcus* spp.), NanoORG (*Cryptophyceae*), and NanoSWS (*Coccolithophoridae*) marked the last phase. After July 10th ($J_d = 191$), the abundance of the PicoRED2 group also increased.

The dynamics of FLR in 2022 exhibited a distinct phenology compared to the 2021 bloom. Initially, the phytoplankton community was progressively dominated by the MicroRED2 group (mainly diatoms), which accounted for approximately 65 % of the total fluorescence on March 23rd ($J_d = 82$; Fig. 4b). This dominance persisted until April 12th ($J_d = 102$). Subsequently, the NanoRED3 group became predominant, culminating in the peak FLR of the bloom on May 10th ($J_d = 130$). This period coincided with the delayed *P. globosa* spring bloom, which occurred later than in 2021. From May 6th ($J_d = 126$), the NanoRED2 group gained prominence, ultimately becoming the most fluorescent group alongside the MicroRED2 group by May 21st ($J_d = 141$). A notable increase in the MicroRED2 group's contribution to total fluorescence was observed through May 26th ($J_d = 146$). In the final phase, starting from June 10th ($J_d = 161$), the NanoSWS and NanoORG groups showed increased contributions to total fluorescence, although this occurred during a period of very low overall FLR values (Fig. 3b).

3.2   Extreme events recorded

Four extreme events were recorded during these two sampling periods: two with sharp wind increases, a desalination event (brackish water inputs), and a heatwave (Fig. 5).
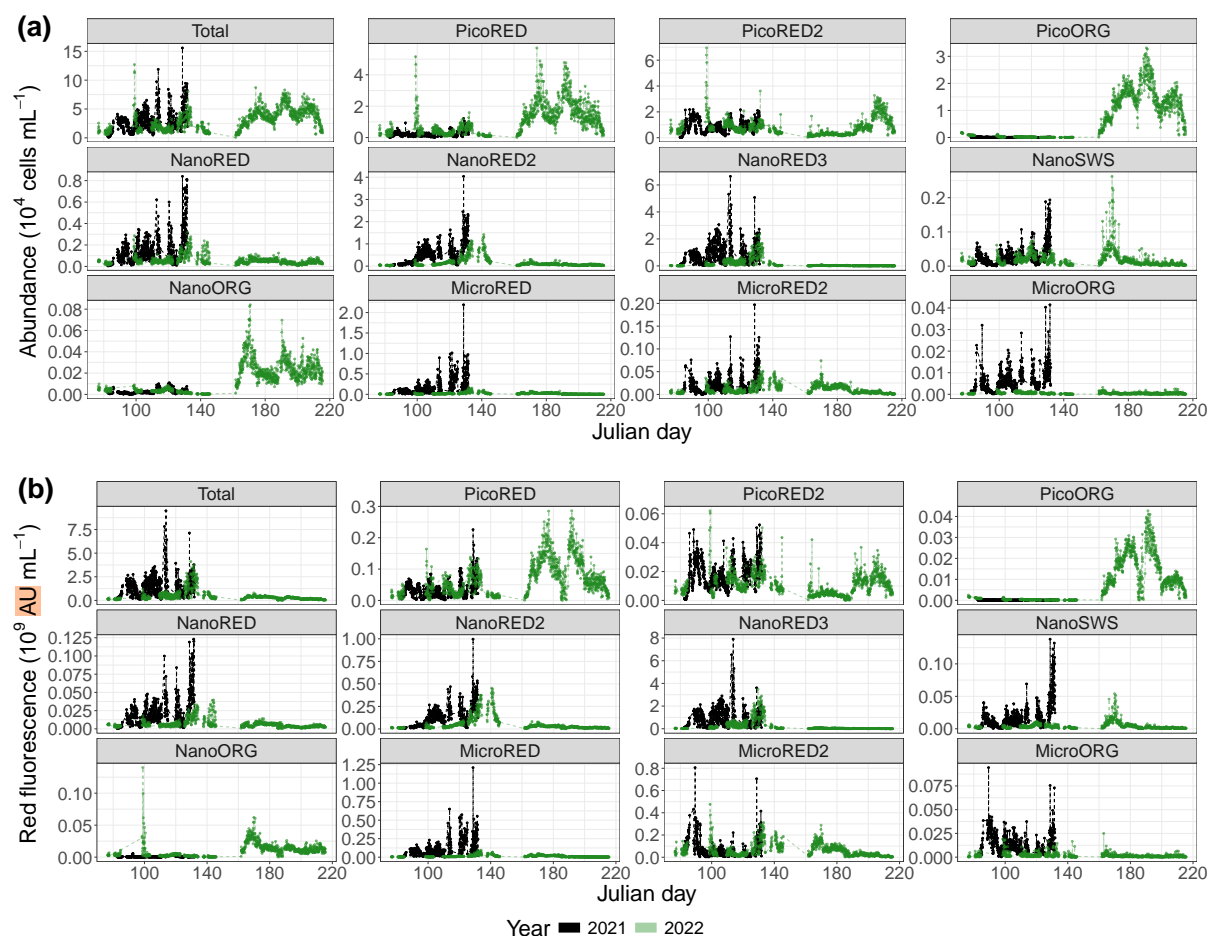
Figure 3. Phytoplankton data recorded with the automated flow cytometer (CytoSub) for each sampled Julian day: (a) phytoplankton abundance and (b) phytoplanktonic red fluorescence (proxy of the chlorophyll *a*). These data are represented in total values and per optically-discriminated PFG. The black line and dots represent 2021 data and the green line and dots represent 2022 data.

The desalination event occurred between April 1st and April 4th 2021 (Fig. 5a,b), with salinity values falling below the 5th percentile (30.73 psu) of the MAREL Carnot salinity dataset. During the initial phase of this event, total phytoplankton abundance decreased, driven primarily by declines in the PicoRED2 and NanoRED3 groups. Subsequently, salinity values dropped even further (< 28 psu), coinciding with peaks in the abundances of the PicoRED, NanoREDs, and MicroRED groups. Notably, the NanoRED3 group exhibited a more rapid change in abundance compared to PicoRED2 during the salinity decline.

The second event observed in 2021 was a breeze with wind speeds ranging from 8 to 20 m s⁻¹ (Fig. 5c,d), exceeding the 90th percentile of MAREL Carnot wind data (16.8 m s⁻¹). During this event, total phytoplankton abundance decreased sharply, particularly during the initial rise in wind speed on May 3rd, and remained low through the larger peak on May 4th. All groups followed the trend of total abundance decline, except for PicoRED2 and MicroRED, which dominated both total abundance
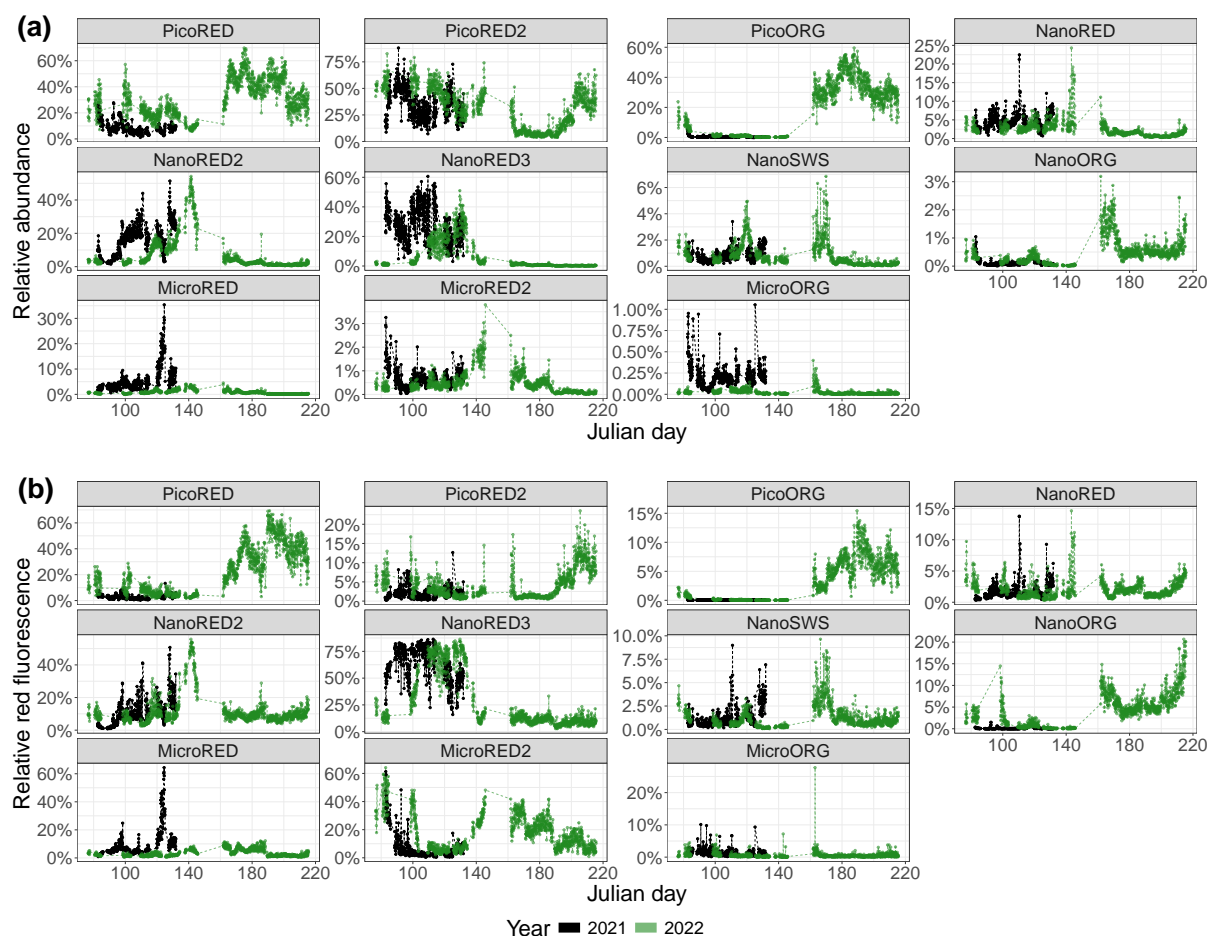
Figure 4. Phytoplankton data recorded for each group with the automated flow cytometer (CytoSub) for each sampled Julian day: (a) PFGs relative abundance and (b) PFGs relative red fluorescence (proxy of the chlorophyll a). The black line and dots represent 2021 data and the green line and dots represent 2022 data.

and fluorescence during this period. After the main wind episode, abundance of NanoRED2 and NanoRED3 increased, accom-
210 panied by high chlorophyll fluorescence, with MicroRED representing more than 60 % of total fluorescence (Fig. 4b), although overall fluorescence remained low (between $0.5 \cdot 10^9$ and $0.6 \cdot 10^9$ AU mL^{-1} on May 3$^{\text{rd}}$).

The third event, a high wind storm (the storm "Diego") in April 2022 (Fig. 5e,f), was marked by a peak in phytoplankton abundance on April 9$^{\text{th}}$. Unfortunately, wind data for this peak were unavailable due to a power outage caused by extreme weather conditions. The PicoRED groups were particularly affected during this event, with observed peaks in their abundance
215 that seemed linked to the wind speeds. In terms of fluorescence, this event appeared to favor the NanoORG group, which reached a relative fluorescence of 15 % (Fig. 4b) during a fluorescence peak, with absolute values close to $1.2 \cdot 10^9$ AU mL^{-1} (Fig. 3b).
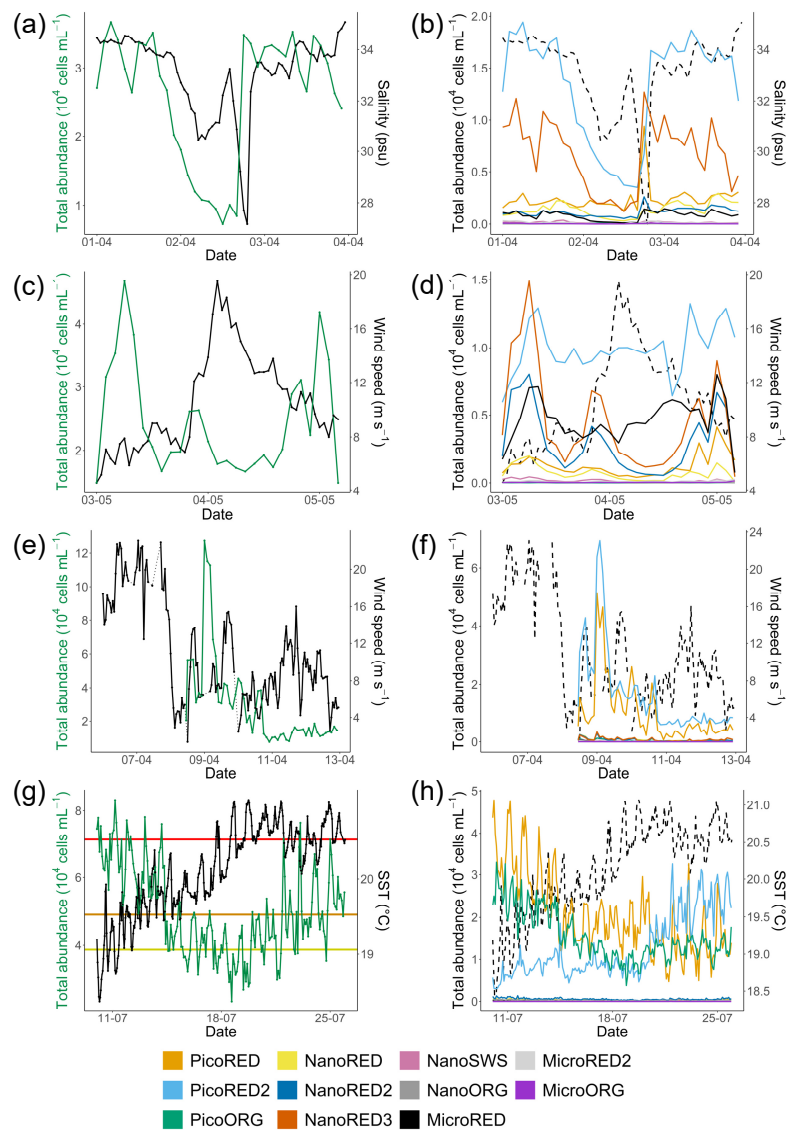
Figure 5. Examples of extreme events recorded on MAREL Carnot station during the study: (a,b) a desalination event in April 2021, (c,d) a high wind speed period in May 2021, (e,f) a strong wind period in April 2022 and (g,h) a high SST event (heatwave) in July 2022. The absolute total abundance are given in the left-column (a,c,e,g; green line) and the absolute abundance for each phytoplankton group are given in the right-column (b,d,f,h; colored lines). The three horizontal lines of the figure (g) represent the 90 % (yellow), 95 % (orange) and 99 % (red) percentile of the SST observations of the MAREL Carnot station between March 24th 2004 and September 30th 2023. The abiotic data (salinity, SST, wind speed) presented here comes from (a,b,e,f,g,h) MAREL Carnot station and (c,d) Météo France (Boulogne-sur-Mer station).

The final event was a marine heatwave (Fig. 5g,h), marked by warm water and high air temperatures in Boulogne-sur-Mer between July 15th and July 20th 2022, with the highest air temperature recorded on July 19th (temperature in a Stevenson

220   screen equal to 39.8 °C according to Météo France data). This event qualifies as a marine heatwave, as the SST reached the 90th percentile for at least five days (Hobday et al., 2016). During this period, phytoplankton abundances decreased as the SST increased, from the 90th (19.06 °C) to the 95th (19.53 °C) and 99th (20.54 °C) percentiles recorded since 2004. This decline was particularly evident in PicoRED and PicoORG groups, which were among the most dominant during this period. PicoORG abundance, for example, halved during the event, and its dynamics showed a strong negative correlation with SST (Pearson

225    $r = -0.78$, p-value $< 2.2 \cdot 10^{-16}$) between July 10th and July 20th. After July 21st, both PicoORG and PicoRED stabilized as SST plateaued. In contrast, PicoRED2 abundance increased during and after the SST peak.

3.3   EMD-LSP

3.3.1   Abundance and FLR

The 2021 time series was analyzed in detail, considering abundance, FLR, and Shannon index data. Seven IMFs were identified,

230   with peak periods ranging from approximately 12.48 hours to 18.9 days (Fig. 6). These periods ($T_{\max}$, see Table 2) corresponded to the highest peaks in their respective LSP. The mean periods of these IMFs ranged from 10.6 hours to 6.1 days (Fig. 7a). The first IMF, C_1, had a mean period of 10.6 hours, with a peak at 12.4 hours, and an additional peak at around 6 hours. This IMF likely corresponds to the current inversion during tides (Jouanneau et al., 2013). The second IMF represents the tidal mode with a mean period of 14.9 hours and a peak near 12.4 hours. The third IMF, C_3, corresponds to two tidal cycles, while the

235   fourth and fifth IMFs, C_4 and C_5, are likely related to tidal cycle impacts at different timescales.

The final two IMFs, C_6 and C_7, align with the periodicity of the neap-spring tide cycle, with periods near the semi-lunar cycle ($T_{\max}$ = 13.2 and 18.9 days, respectively). The residual dynamics showed an overall increase in total phytoplankton abundance during the bloom period, with fluctuations following the lunar cycle. Peaks in abundance corresponded to spring tides, while troughs aligned with neap tides.

240   Notably, the periods of the different IMFs follow a power law: $\overline{T_i} \sim \gamma^i$. The exponent γ was found to be 1.62, which is lower than the value of 2 typically observed for fractional Gaussian noise (Flandrin et al., 2004; Flandrin and Gonçalvès, 2004) or turbulent time series (Huang et al., 2008). This indicates that the period of each mode is approximately 1.62 times longer than that of the preceding mode.

The loss of variance, V_i^{lost}, is shown in Fig. 7b for the first example, illustrating the loss of information after removing each

245   IMF from the raw abundance signal. The explained variance decreases with the removal of each IMF, with the loss following a logarithmic pattern: $V_i^{\text{lost}} \sim 43.79 \cdot \log_{10}(\overline{T_i})$.

The results for all the studied time series (abundance, FLR, Shannon index) are summarized in Table 2. Each time series exhibited between 7 and 10 distinct IMFs with mean periods ranging from approximately 9 hours and 11 days. Notably, the variance loss increased sharply with the different modes, particularly for the 2021 abundance and FLR time series, where

250   tidal modes accounted for at least 62 % of the total variance. The γ values ranged from 1.45 to 1.62, lower than the value
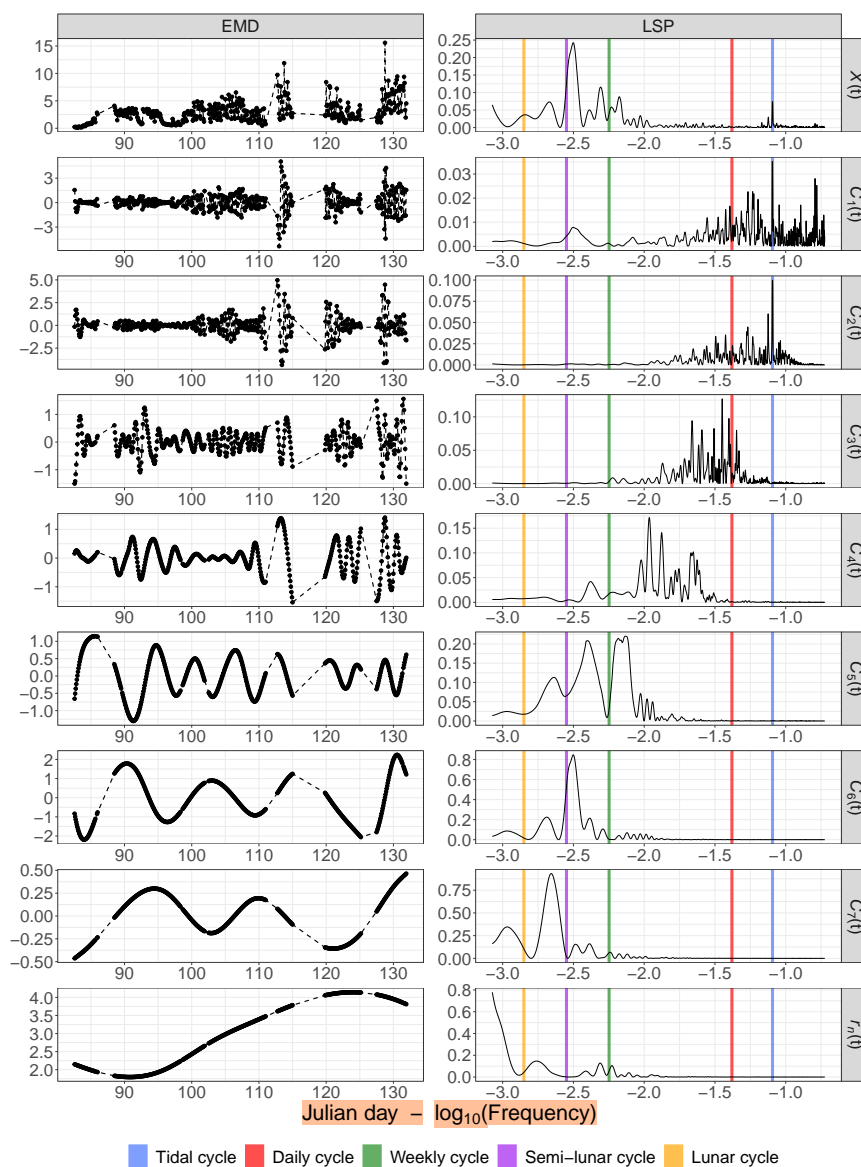
Figure 6. Decomposition of the 2021 total phytoplankton abundance data using the Empirical Mode Decomposition (EMD; left part) and the associated Lomb-Scargle Periodograms (LSP; right part) for the raw time series $X(t)$, for each IMF $C_i(t)$ and for the residue $r_n(t)$. The EMD x-axis represents the Julian days and the y-axis represents the abundance values (cells mL^{-1}). The LSP x-axis represents the decimal logarithm ($\log_{10}$) of the frequency (in h^{-1}) and the y-axis represents the normalized power.

of 2 typically found in turbulent and Gaussian time series, indicating the presence of many high frequency modes. Overall, a significant proportion of the variability was lost quickly, with at least 72 % of the variance disappearing for time series without modes with mean periods between 4 and 11 days. This suggests that most phytoplankton variability occurred at
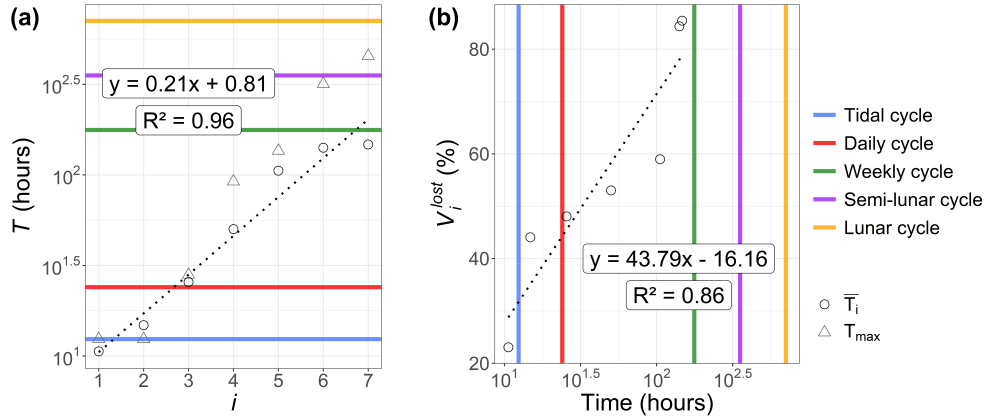
Figure 7. Results obtained from the EMD-LSP analysis for the 2021 phytoplankton abundance time series: (a) the mean period ($\overline{T_i}$) and maximum peak period ($T_{\max}$) of each IMF $C_i(t)$ and (b) the percentage of variance explained for different timescales based on the mean periods of these IMFs. The black dashed lines represent the linear regressions estimated. The associated formula and coefficient of determination R^2 are displayed on the respective figure.
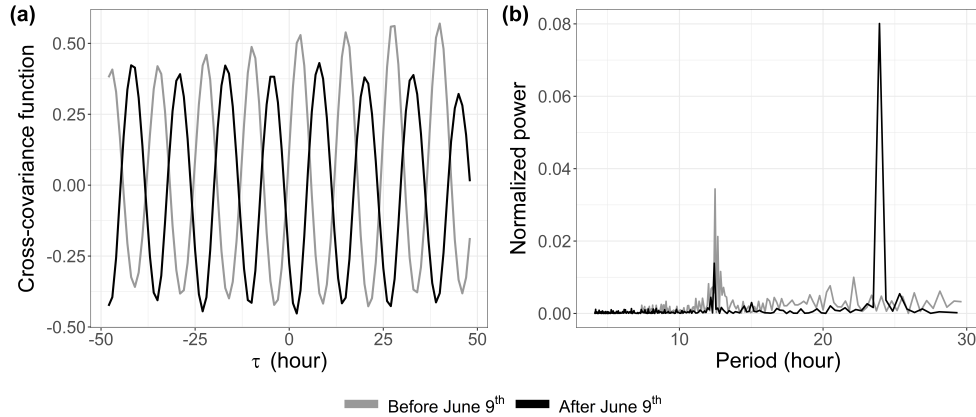
Figure 8. Short timescales observations for the 2022 phytoplankton abundance data before and after June 9th: (a) cross-covariance functions between the water height data (REFMAR data; SHOM, 2024) and the abundance data and (b) Lomb-Scargle Periodograms of the abundance data.

low timescales. Additionally, according to the Nyquist-Shannon theorem, fluctuations at frequencies f_e cannot be captured

255 by sampling frequencies lower than $2/f_e$. Thus, a time resolution of at least 5 hours is necessary to avoid losing this high frequency modal variability.

A link between phytoplankton dynamics and the tidal cycle was observed through cross-correlation with the water height time series. This analysis revealed a shift in the short timescale dynamics of phytoplankton abundance in 2022, occurring after June 9th (Fig. 8a). For the 2021 data and the early part of the 2022 data, phytoplankton abundance (and FLR, see Appendix A)

Table 2. Indicators estimated from EMD-LSP for each IMF $C_i(t)$ of the abundance, red fluorescence (FLR) and Shannon index H' time series of 2021 and 2022: the period of the maximum peak of the LSP $T_{\max}$ (days), the mean period $\overline{T_i}$ (days), the loss of explained variance in the time series after removing the i first IMFs V_i^{lost} (%) and the γ value for which $\overline{T_i} \sim \gamma^i$.

Year											
		2021						2022			
Time series (Units)	i	$T_{\max}$ (d)	$\overline{T_i}$ (d)	V_i^{lost} (%)	γ	Time series (Units)	i	$T_{\max}$ (d)	$\overline{T_i}$ (d)	V_i^{lost} (%)	γ
Abundance	1	0.52	0.44	23.05	1.62	Abundance	1	0.52	0.49	2.06	1.45
(cell mL⁻¹)	2	0.52	0.62	44.06		(cell mL⁻¹)	2	1.00	0.69	5.34	
	3	1.17	1.07	48.05			3	1.00	1.09	7.57	
	4	3.83	2.09	53.02			4	3.54	2.52	8.80	
	5	5.66	4.40	58.97			5	10.96	4.07	10.19	
	6	13.23	5.89	84.36			6	15.62	10.53	17.07	
	7	18.90	6.13	85.44			7	65.57	6.19	61.14	
	-	-	-	-			8	63.47	7.46	71.62	
	-	-	-	-			9	42.64	5.96	90.18	
FLR	1	0.48	0.77	33.08	1.51	FLR	1	0.52	0.44	9.03	1.55
(AU mL⁻¹)	2	0.52	0.65	62.32		(AU mL⁻¹)	2	0.52	0.57	16.53	
	3	1.50	1.15	66.54			3	1.93	1.31	22.26	
	4	3.22	1.93	70.74			4	2.13	2.12	25.25	
	5	6.59	3.97	74.89			5	16.22	3.48	28.66	
	6	13.02	5.48	89.69			6	26.63	8.82	55.34	
	7	6.05	3.34	93.28			7	57.20	6.11	66.94	
	-	-	-	-			8	55.16	6.86	72.14	
$\exp(H'_{\text{abundance}})$	1	0.60	0.38	10.44	1.55	$\exp(H'_{\text{abundance}})$	1	0.26	0.45	0.17	1.32
	2	0.52	0.62	18.67			2	0.53	0.69	0.31	
	3	1.07	1.10	22.37			3	1.59	1.07	0.39	
	4	2.48	1.96	24.62			4	5.17	2.10	0.46	
	5	3.29	2.58	30.75			5	10.24	4.74	0.84	
	6	12.52	5.04	35.15			6	42.64	5.75	1.57	
	7	24.30	9.20	50.44			7	69.50	5.07	23.80	
	8	15.56	5.18	80.09			8	45.28	3.49	70.36	
	-	-	-	-			9	39.83	5.60	75.74	
	-	-	-	-			10	41.49	4.30	91.36	
$\exp(H'_{\text{FLR}})$	1	0.53	0.46	20.29	1.35	$\exp(H'_{\text{FLR}})$	1	0.26	0.44	6.51	1.45
	2	0.94	0.63	32.41			2	0.52	0.67	11.34	
	3	2.36	1.24	38.54			3	1.00	1.09	14.08	
	4	1.72	2.32	43.32			4	2.64	2.13	16.41	
	5	5.03	4.24	49.13			5	4.97	3.04	18.64	
	6	10.39	5.44	51.96			6	11.75	4.96	24.45	
	7	10.61	5.57	56.44			7	28.72	10.67	48.87	
	8	22.02	6.23	64.61			8	29.14	6.95	78.79	
	9	6.01	3.10	65.79			9	39.71	7.53	84.34	
	-	-	-	-			10	42.90	9.48	86.22	

showed a positive correlation with water height. However, after June 9th in 2022, the relationship became negative. Furthermore, the LSP revealed a shift in dynamics before and after June 9th. A high peak was observed at 12 hours before June 9th,
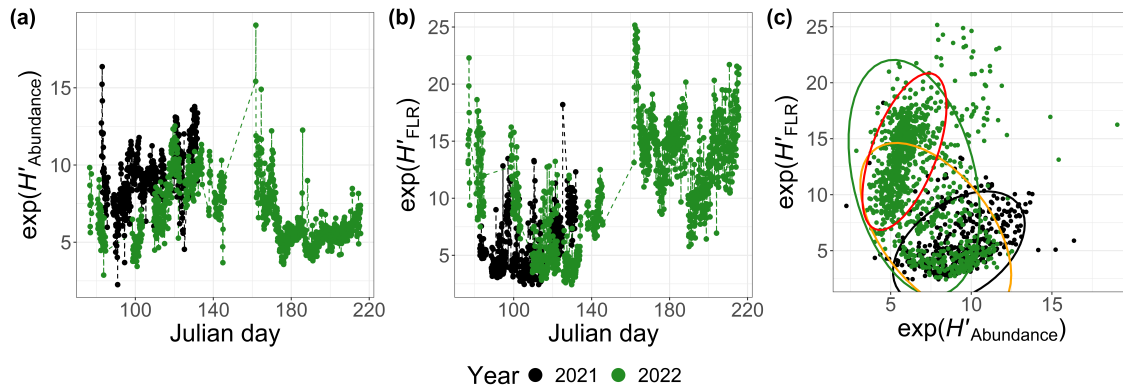
Figure 9. Exponential values of Shannon index H' calculated for 2021 and 2022 based on (a) the abundance ($H'_{\mathrm{Abundance}}$) and (b) the FLR (H'_{FLR}) in function of the Julian day and (c) comparison of these two quantities. The ellipses represent the t distributions with a 95 % confidence interval. The orange ellipse take into account 2022 data before June 9th and the red one takes into account that after June 9th.
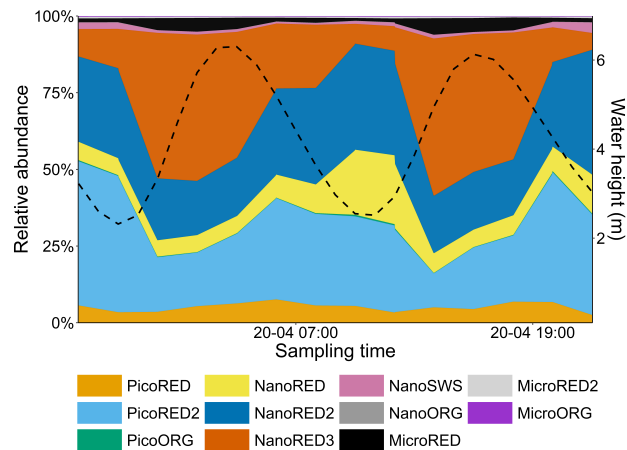
Figure 10. Relative abundance of each PFG (colored area) and water height (black dashed line; SHOM, 2024) between April 19th and 21st, 2021.

which persisted but with reduced power after this date. A new peak appeared at 24 hours, highlighting the changing temporal variability of the environmental forcing on phytoplankton communities.

3.3.2 Shannon diversity index H'

265 A difference was observed in the dynamics of the diversity index, $\exp(H')$, when calculated from abundance ($H'_{\mathrm{abundance}}$; Fig. 9a) versus FLR (H'_{FLR}; Fig. 9b). In 2022, the diversity index based on abundance decreased after $J_d = 160$ (June 9th), while the FLR-based index increased during the same period (Fig. 9c). This shift can be attributed to the dominance of pico-

organisms during the summer bloom, which have a lower chlorophyll *a* content and, therefore, contribute less to the total FLR. In contrast, $H'_{\text{abundance}}$ peaked during the *P. globosa* bloom, while H'_{FLR} showed an opposite trend.

270 The Shannon index time series exhibited similar IMFs to those observed for abundance and FLR, with notable high frequency variations and the presence of tidal modes ($T_{\max} \simeq 0.52$ day). These tidal modes likely reflect the varying responses of different PFGs to tidal forces, with community composition evolving during each tidal cycle (Fig. 10). The γ values ranged from 1.32 to 1.55 (Table 2), indicating the dominance of high frequency modes at short timescales, which accounted for at least 65 % of the variability. These findings underscore the multi-scale dynamics of the system, with high frequency variations playing a
275 significant role in shaping phytoplankton community assemblages.

4 Discussion

In this study, an automated flow cytometer was deployed at the MAREL Carnot fixed automated measuring station to monitor phytoplankton at high frequency. The goal was to observe and describe the variations in phytoplankton time series across several timescales, ranging from hourly events (e.g., extreme events, tidal forcing) to monthly events (e.g., phenologies). It was
280 hypothesized that these multi-scale events influence phytoplankton communities.

4.1 Weekly-scale dynamics

In spring 2021, a significant bloom of NanoRED groups was observed, emerging phenologically in an environment where MicroRED2 (large diatoms and colonies) and PicoREDs (picoeukaryotes) dominated in terms of FLR and abundance, respectively. The increasing abundance of NanoRED groups was mostly due to the haptophyte *P. globosa*, which could be
285 characterized through imaging (using the "Micro-Photos" protocol) and corroborated by previous studies (Rutten et al., 2005; Guiselin, 2010; Bonato et al., 2015).

This phenological shift, with a transition from diatoms (MicroRED2) to *P. globosa* (NanoREDs), was also observed in 2022 and has been previously documented in the study area (Breton et al., 2000; Guiselin, 2010; Grattepanche et al., 2011; Lefebvre et al., 2011; Hernández-Fariñas et al., 2014; Genitsaris et al., 2015; Lefebvre and Dezécache, 2020; Houliez et al.,
290 2023). The *P. globosa* spring bloom is known to occur when abiotic conditions are favorable, such as nutrient availability and light conditions (e.g., Gentilhomme and Lizon, 1997; Lancelot et al., 2011; Lefebvre et al., 2011; Lefebvre and Dezécache, 2020; Breton et al., 2022). More specifically, *P. globosa* became predominant following the depletion of Si(OH)_4 and PO_4^{3-} (Fig. 11a), which were consumed during the diatom bloom, as observed in other studies (Karasiewicz et al., 2018).

The abundance of the MicroRED group was also notably high during the spring bloom of 2021. This group, composed of
295 pennate diatoms optically similar to the *Pseudo-Nitzschia* complex (likely *P. delicatissima* in this season; Delegrange et al., 2018), was confirmed through the "Micro-Photo" protocol. The presence of MicroREDs could be linked to the high abundance of *P. globosa*, as a commensal symbiotic relationship between these two species has been described (epibiosis; Sazhin et al., 2007).
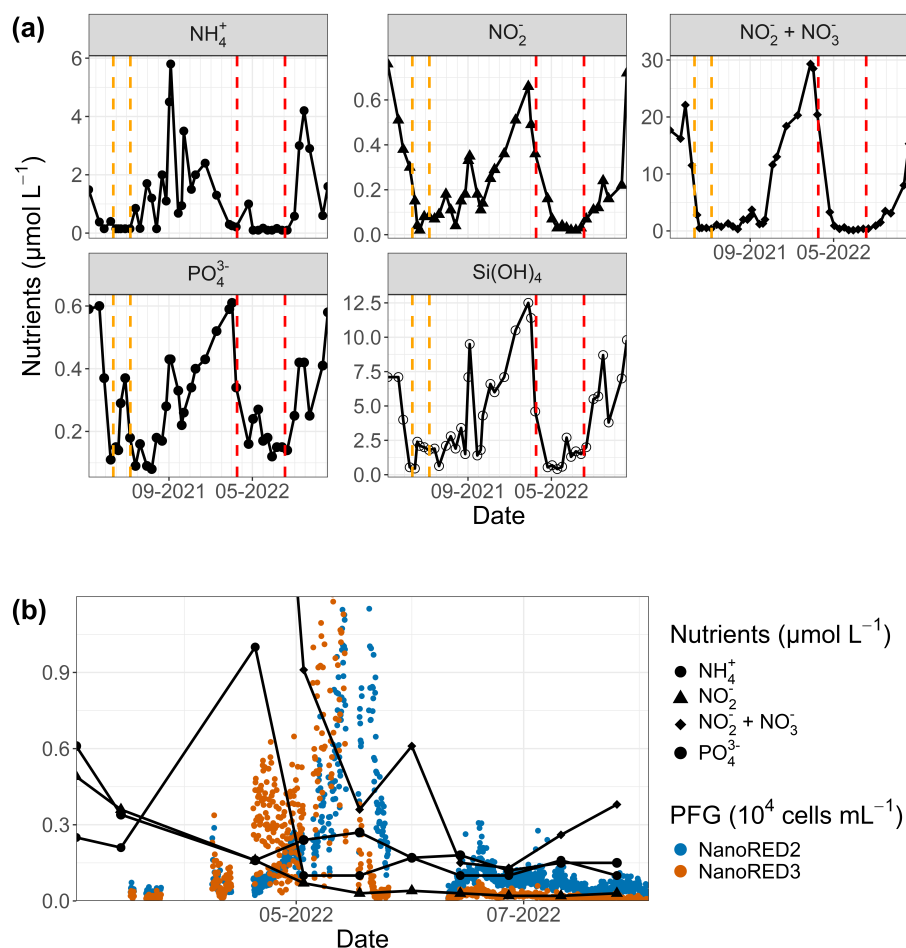
Figure 11. SRN nutrients data (Lefebvre et al., 2024) at the 'Boulogne 1' station: (a) for 2021 and 2022 and (b) for the 2022 study period. The two study periods are highlighted in (a) by the dashed lines (orange for 2021 and red for 2022). The NanoRED2 and NanoRED3 2022 abundance data are represented in (b) by the colored dots.

A similar spring bloom of NanoREDs was observed in 2022, although it was less pronounced in terms of FLR compared
300 to 2021. This could be attributed to the longer persistence of nano- and microplankton cells in 2021, which may have been
facilitated by higher PO_4^{3-} concentrations during that year (Fig. 11a).

In 2022, the decline of the NanoREDs bloom was evident, unlike in 2021, when measurements were ended earlier than in
2022. As the NanoREDs bloom faded, other groups began to increase, including coccolithophorids (NanoSWS), cryptophytes
(NanoORG), diatoms (MicroRED2) in terms of FLR, and particularly cyanobacteria (PicoORG) and chlorophyll picoeukary-
305 otes (PicoREDs) in terms of abundance. The dominance of these smaller cells following the spring bloom can be explained by
their higher competitiveness in nutrient-poor environments (Litchman et al., 2007). Similar successions have been observed in
the region and are partly explained by the physico-chemical conditions of the ecosystem (Bonato et al., 2016).

Furthermore, a succession between the NanoRED3 and NanoRED2 groups was also apparent at the end of the spring bloom (Fig. 11b). As the abundance of NanoRED3 declined, NanoRED2 became more dominant for a period. This phenomenon, also

310 observed at the end of the 2021 data recording (although less clearly), may reflect competition between different life stages of *P. globosa*. The flagellated form of *P. globosa* (NanoRED2) is more competitive in nutrient-limited environments compared to its colonial cell form (NanoRED3; Rousseau et al., 1994; Peperzak et al., 2000). As nutrients were consumed, the abundant form of this haptophyte shifted, revealing a long-term phenology driven by the gradual depletion of nutrient stocks during the spring and early summer (visible in Fig. 11a; Gentilhomme and Lizon, 1997; Lancelot et al., 2011; Lefebvre et al., 2011).

315 **4.2 Extreme events**

High frequency studies enable the detection of rapid and intense events that cannot be captured with low-frequency sampling typical of long-term monitoring networks. These events can have significant ecological impacts, as different phytoplankton communities respond differently to environmental changes. This was evident during two high-wind-speed events, which had contrasting effects on phytoplankton abundance.

320 In one instance, a strong wind event between May 3rd and 6th, 2021, promoted the dominance of the MicroRED PFG (comprising the *Pseudo-Nitzschia* complex). During this period, all NanoRED groups decreased, while MicroRED groups increased. This shift could be explained by the resuspension of cells that had previously settled, supported by the observed increase in turbidity during this time (based on MAREL Carnot data, not shown here). Additionally, the breakdown of *P. globosa* colonies, possibly due to their commensal relationship with MicroREDs (Sazhin et al., 2007), could have contributed to this increase.

325 Following the wind event, NanoRED groups went up, likely due to the release of *P. globosa* colonial forms. Interestingly, pico-organisms (PicoRED and PicoRED2) did not appear to be significantly affected by this storm. In contrast, a high-wind-speed event in 2022 triggered a peak in the abundance of PicoRED groups. The difference in the effects of the two events may be attributed to the wind direction: during the 2021 event, the wind was blowing from 225° (South-West), while during the 2022 event, the wind came from 350° (North-North-West) shortly before the PicoREDs abundance peak (as the weather station

330 data ceased on April 9th). Wind direction is an important factor for particle transport in the harbor, and this shift could explain the contrasting responses of the phytoplankton groups (Jouanneau et al., 2013).

Additionally, the marine heatwave and low-salinity events highlighted in Sect. 3.2 also induced different responses among phytoplankton communities, with significant shifts in the assemblages occurring over just a few hours. For instance, the PicoRED2 PFG appeared to be favored during the marine heatwave compared to other pico-plankton groups. During the 2021

335 low-salinity event, two distinct peaks of low salinity were observed on the same day, yet the communities responded differently at each peak. These observations underscore the complexity and non-linearity of phytoplankton community responses to extreme events, even within the same area. Further high-frequency observations are crucial to fully understanding the effects of such events on pelagic phytoplankton ecosystems, as emphasized by previous studies (e.g., Barrillon et al., 2023; Röthig et al., 2023).

4.3 High-frequency multi-scale dynamics

The time series analyzed revealed a multi-scale dynamics, ranging from hours to several days, with high-frequency fluctuations (9 hours to 11 days) explaining at least 65 % of the total phytoplankton variance. Notably, tidal modes contributed significantly to phytoplankton dynamics, as observed in other regions for chlorophyll *a* (Blauw et al., 2012). The high tidal range in our study area, along with temporal heterogeneity and patchiness of phytoplankton, likely drives this variability in total abundance and total FLR (Seuront et al., 1996; Seuront, 2005). Additionally, the neap-spring tidal cycle influenced the data, with increased tidal range during spring tides amplifying phytoplankton variability. This effect is linked to the coastal river's structure, where a vertical front during spring tides limits exchanges between coastal and offshore waters, isolating phytoplankton blooms near the coast, especially in westerly winds regime.

High-frequency dynamics also impacted community composition, with shifts observable in the Shannon diversity index, reflecting changes at multiple ecological scales. The tidal mode influenced this index, representing up to 20 % of the total variability, highlighting the diverse influence of hydrological forcing on different PFGs. This indicates that multi-scale dynamics and high-frequency fluctuations affect phytoplankton ecology at the community level.

Furthermore, high-frequency forcing effects were not stable over time. After June 9th, 2022, a shift was observed in the relationship between phytoplankton abundance and water height, alongside the emergence of a new 24-hour periodicity. This change could be attributed to a different life cycle of dominant picoorganisms compared to nano- and microphytoplankton, as picoeukaryotes (PicoRED) and cyanobacteria (PicoORG) predominated during this period. Previous studies have shown a strong link between SST and cyanobacterial growth in waters with an annual mean SST below 14 °C (Li, 1998). The EEC, with an annual mean SST of 12.69 °C (based on MAREL Carnot data), aligns with these findings. We observed higher picoorganism abundance at night (when SST is lower) and lower abundance during the day (when SST is higher; Fig. 12) as it has already been observed in *Synechococcus* dynamics (Xiu-ren and Vaulot, 1996; Sosik et al., 2003). Grazing effects could also explain in part these patterns, as noted by Xiu-ren and Vaulot (1996). Moreover, this daily cycle was also observed in the PicoORG and PicoRED FWS per cell time series (a proxy for cell size; Fig. 12), consistent with the fact that cells increase in size before division (André et al., 1999). This kind of daily dynamics for the FWS per cell was also observed for some groups (as NanoRED3) in 2021 and for the data of 2022 before June 9th, but not on the abundance data.

SST plays a crucial role in driving picoeukaryotes and cyanobacterial dynamics, both periodically (e.g., daily cycles) and non-periodically (e.g., marine heatwaves). This link is consistent with previous studies (Chen et al., 2014; Hunter-Cevera et al., 2020). As EEC coastal waters warm due to global change (+1 °C over the past 10 years, with a projected +3.34±0.88 °C by 2100; Hubert et al., 2024; Tinker et al., 2024), monitoring the long-term high-frequency dynamics of picoorganisms, in addition to other size-classes, is of the must importance. These organisms are critical to pelagic food webs and biogeochemical cycles (Xiu-ren and Vaulot, 1996), and understanding how they will respond to warming and associated extreme events is crucial.
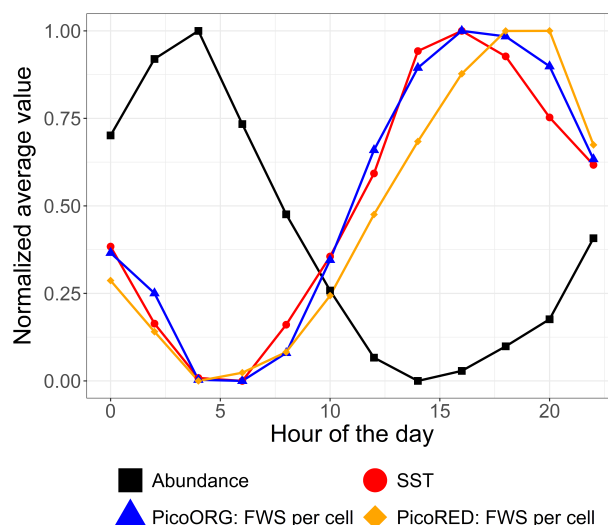
Figure 12. Mean average abundance, SST and cell size proxy (FWS) of the PicoORG (*Synechococcus* spp. like) and PicoRED (picoeukaryotes) groups normalized (between 0 and 1 using the following formula: $\frac{y - y_{\min}}{y_{\max} - y_{\min}}$) for each hour of the day, for the 2022 data after June 9th.

5 Conclusions

This study characterizes the multi-scale dynamics of phytoplankton during the springs of 2021 and 2022 off the Liane estuary, and the Boulogne-sur-Mer coastal area in the Eastern English Channel. We evidenced the seasonal successions between key Phytoplankton Functional Groups (PFGs), particularly between MicroRED groups (mostly diatoms) and NanoRED (mostly

375   haptophytes of the genus *Phaeocystis globosa*). Using the Empirical Mode Decomposition and Lomb-Scargle Periodogram method, we identified various modal fluctuations across different temporal scales in phytoplankton abundance, red fluorescence (proxy of chlorophyll *a*), and the Shannon diversity index, highlighting the complex dynamics of population assemblages.

Our findings reveal that much of the variability in these time series occurs at short time scales, with modes on the order of a few days. This indicates that low-frequency sampling may miss significant dynamics in phytoplankton communities. We also

380   observed that these multi-scale fluctuations do not stabilize over time, particularly during the seasonal shifts in community composition, such as the dominance of picoorganisms in summer 2022 when sea surface temperature became a major driver of abundance.

The study's limited duration, constrained by the system's design, suggests the need for longer-term monitoring of PFGs, coupled to HF measurements of more abiotic variables as nutrients, to assess whether high-frequency fluctuations become less

385   significant over larger temporal scales (e.g., inter-annual variations) in the context of global change and changing anthropogenic pressures, to better understand the mechanisms of their impact on the whole size-range of main marine primary producers. Additionally, incorporating higher trophic levels, such as zooplankton, could offer insights into top-down control mechanisms, which were not fully addressed here.

Overall, this study confirms the interest and big potential of combining automated flow cytometry with fixed buoys for
high-frequency monitoring of marine ecosystems, though the system's design requires adaptation for long-term use. Given the
increasing frequency of extreme events like storms, estuarine loads, and heatwaves in coastal areas, automated monitoring,
coupled with robust statistical analyses, is crucial for understanding phytoplankton variability and its impact on marine food
webs and biogeochemical cycles. This approach can provide valuable data for models predicting changes in ecosystem structure
and function.

Appendix A: Cross-covariance function of 2022 FLR data

The cross-covariance functions between the water height data (REFMAR data; SHOM, 2024) and the FLR data before and
after June 9th 2022 are displayed in Fig. A1. An inversion of the link between the two time series was observed, as it was also
the case between the water height and the abundance data (Fig 8). This link was yet less important after June 9th, as the area
was dominated by picoorganisms.
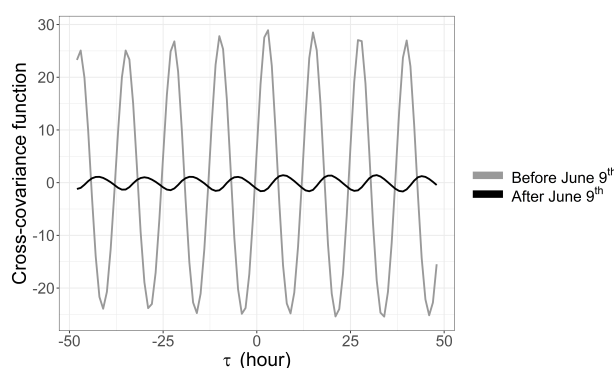
Figure A1. Cross-covariance functions between the water height data (REFMAR data; SHOM, 2024) and the FLR data before and after
June 9th 2022.

Code and data availability. The cytometric data (https://doi.org/10.17882/104948; Robache et al., 2025), the SRN (nutrients) data (https://doi.org/10.17882/50832; Lefebvre et al., 2024), and the MAREL Carnot data (https://doi.org/10.17882/39754; MAREL Carnot, 2024) are accessible from SEANOE portal. The REFMAR data are accessible from SHOM portal (Boulogne-sur-Mer station: http://doi.org/10.17183/REFMAR#111; SHOM, 2024). EMD-LSP analysis have been performed using the 'EMD' (https://doi.org/10.32614/CRAN.package.EMD; Kim and Oh, 2009) and 'lomb' (https://doi.org/10.32614/CRAN.package.lomb; Ruf, 1999) R software packages. All the plots have been made using the 'tidyverse' (https://doi.org/10.32614/CRAN.package.tidyverse) R packages, and more especially the 'ggplot2' (https://doi.org/10.32614/CRAN.package.ggplot2) package (Wickham et al., 2019).

Author contributions. This work was conceptualized by LFA, KR, CG, AE, and ZH in association to AL, JVF and MR. The fieldwork was carried out by KR, JVF, CG, AE, ZH, VC, FV, YA, LB, and LFA. KR performed the code and the analysis. KR interpreted the results with the help of ZH, CG, AE, APL, FGS and LFA. KR and ZH wrote the first draft and all authors edited the final version. LFA and FGS secured
410   the funding acquisition and supervised KR.

Competing interests. The authors declare that no competing interests are present.

Acknowledgements. We would like to thank Noël Filiattre and Christophe Routtier, the crew of the vessel *Sepia II*. We would also like to thank Benoît Chedot for its precious help during 2022 deployment.

Financial support. This work has been financially supported by the European Union (European Regional Development Fund), the French
415   State, the French Region Hauts-de-France and Ifremer, in the framework of the projects CPER MARCO 2015-2021 and IDEAL 2021-2027. The H2020 JERICO S3 project supported the deployment strategy of automated sensors, the SNO COAST-HF allowed the coupling of the CytoSub to the MAREL Carnot automated monitoring station, and the IR ILICO funded KR Master's thesis. This work was also supported by ongoing projects Horizon EU project OBAMA-NEXT and the "Programme Prioritaire de Recherche" (PPR) RiOMar funded by the French National Research Agency (France 2030 grant no. ANR-22-POCE-0006). ZH is co-funded by the French Region Hauts-de-France and by
420   an Université du Littoral Côte d'Opale (ULCO) PhD grant. AE was supported by an ULCO and by the graduate school IFSea (France 2030 grant no. ANR-21-EXES-0011) post-doctoral fellowship.

References

André, J.-M., Navarette, C., Blanchot, J., and Radenac, M.-H.: Picophytoplankton Dynamics in the Equatorial Pacific: Growth and Grazing Rates from Cytometric Counts, Journal of Geophysical Research: Oceans, 104, 3369–3380, https://doi.org/10.1029/1998JC900005, 1999.

Bar-On, Y. M. and Milo, R.: The Biomass Composition of the Oceans: A Blueprint of Our Blue Planet, Cell, 179, 1451–1454, https://doi.org/10.1016/j.cell.2019.11.018, 2019.

Bar-On, Y. M., Phillips, R., and Milo, R.: The Biomass Distribution on Earth, Proceedings of the National Academy of Sciences, 115, 6506–6511, https://doi.org/10.1073/pnas.1711842115, 2018.

Barrillon, S., Fuchs, R., Petrenko, A. A., Comby, C., Bosse, A., Yohia, C., Fuda, J.-L., Bhairy, N., Cyr, F., Doglioli, A. M., Grégori, G., Tzortzis, R., d'Ovidio, F., and Thyssen, M.: Phytoplankton Reaction to an Intense Storm in the North-Western Mediterranean Sea, Biogeosciences, 20, 141–161, https://doi.org/10.5194/bg-20-141-2023, 2023.

Bertin, S., Sentchev, A., and Alekseenko, E.: Fusion of Lagrangian Drifter Data and Numerical Model Outputs for Improved Assessment of Turbulent Dispersion, Ocean Science, 20, 965–980, https://doi.org/10.5194/os-20-965-2024, 2024.

Blauw, A. N., Benincà, E., Laane, R. W. P. M., Greenwood, N., and Huisman, J.: Dancing with the Tides: Fluctuations of Coastal Phytoplankton Orchestrated by Different Oscillatory Modes of the Tidal Cycle, PLOS ONE, 7, e49 319, https://doi.org/10.1371/journal.pone.0049319, 2012.

Bonato, S., Christaki, U., Lefebvre, A., Lizon, F., Thyssen, M., and Artigas, L. F.: High Spatial Variability of Phytoplankton Assessed by Flow Cytometry, in a Dynamic Productive Coastal Area, in Spring: The Eastern English Channel, Estuarine, Coastal and Shelf Science, 154, 214–223, https://doi.org/10.1016/j.ecss.2014.12.037, 2015.

Bonato, S., Breton, E., Didry, M., Lizon, F., Cornille, V., Lécuyer, E., Christaki, U., and Artigas, L. F.: Spatio-Temporal Patterns in Phytoplankton Assemblages in Inshore–Offshore Gradients Using Flow Cytometry: A Case Study in the Eastern English Channel, Journal of Marine Systems, 156, 76–85, https://doi.org/10.1016/j.jmarsys.2015.11.009, 2016.

Breton, E., Brunet, C., Sautour, B., and Brylinski, J.-M.: Annual Variations of Phytoplankton Biomass in the Eastern English Channel: Comparison by Pigment Signatures and Microscopic Counts, Journal of Plankton Research, 22, 1423–1440, https://doi.org/10.1093/plankt/22.8.1423, 2000.

Breton, E., Goberville, E., Sautour, B., Ouadi, A., Skouroliakou, D.-I., Seuront, L., Beaugrand, G., Kléparski, L., Crouvoisier, M., Pecqueur, D., Salmeron, C., Cauvin, A., Poquet, A., Garcia, N., Gohin, F., and Christaki, U.: Multiple Phytoplankton Community Responses to Environmental Change in a Temperate Coastal System: A Trait-Based Approach, Frontiers in Marine Science, 9, https://doi.org/10.3389/fmars.2022.914475, 2022.

Brylinski, J.-M., Lagadeuc, Y., Gentilhomme, V., Dupont, J.-P., Lafite, R., Dupeuble, P.-A., Huault, M.-F., Auger, Y., Puskaric, E., Wartel, M., and Cabioch, L.: Le "Fleuve Cotier": Un Phénomène Hydrologique Important En Manche Orientale. Exemple Du Pas-de-Calais, Oceanologica Acta, Special issue, https://archimer.ifremer.fr/doc/00268/37874/, 1991.

Chen, B., Liu, H., Huang, B., and Wang, J.: Temperature Effects on the Growth Rate of Marine Picoplankton, Marine Ecology Progress Series, 505, 37–47, https://doi.org/10.3354/meps10773, 2014.

Chiswell, S. M., Calil, P. H., and Boyd, P. W.: Spring Blooms and Annual Cycles of Phytoplankton: A Unified Perspective, Journal of Plankton Research, 37, 500–508, https://doi.org/10.1093/plankt/fbv021, 2015.

Cloern, J. E., Foster, S. Q., and Kleckner, A. E.: Phytoplankton Primary Production in the World's Estuarine-Coastal Ecosystems, Biogeosciences, 11, 2477–2501, https://doi.org/10.5194/bg-11-2477-2014, 2014.

Crossland, C. J., Baird, D., Ducrotoy, J.-P., Lindeboom, H., Buddemeier, R. W., Dennison, W. C., Maxwell, B. A., Smith, S. V., and Swaney,
460   D. P.: The Coastal Zone — a Domain of Global Interactions, in: Coastal Fluxes in the Anthropocene: The Land-Ocean Interactions in the
        Coastal Zone Project of the International Geosphere-Biosphere Programme, edited by Crossland, C. J., Kremer, H. H., Lindeboom, H. J.,
        Marshall Crossland, J. I., and Le Tissier, M. D. A., Global Change — The IGBP Series, pp. 1–37, Springer, Berlin, Heidelberg, ISBN
        978-3-540-27851-1, 2005.

Cunningham, A. and Buonnacorsi, G. A.: Narrow-Angle Forward Light Scattering from Individual Algal Cells: Implications for Size and
465   Shape Discrimination in Flow Cytometry, Journal of Plankton Research, 14, 223–234, https://doi.org/10.1093/plankt/14.2.223, 1992.

Delegrange, A., Lefebvre, A., Gohin, F., Courcot, L., and Vincent, D.: *Pseudo-Nitzschia* Sp. Diversity and Seasonality in the Southern
        North Sea, Domoic Acid Levels and Associated Phytoplankton Communities, Estuarine, Coastal and Shelf Science, 214, 194–206,
        https://doi.org/10.1016/j.ecss.2018.09.030, 2018.

Dubelaar, G. B. J. and Gerritzen, P. L.: CytoBuoy: A Step Forward towards Using Flow Cytometry in Operational Oceanography, Scientia
470   Marina, 64, 255–265, https://doi.org/10.3989/scimar.2000.64n2255, 2000.

Dubelaar, G. B. J. and Jonker, R. R.: Flow Cytometry as a Tool for the Study of Phytoplankton, Scientia Marina, 64, 135–156,
        https://doi.org/10.3989/scimar.2000.64n2135, 2000.

Dubelaar, G. B. J., Geerders, P. J. F., and Jonker, R. R.: High Frequency Monitoring Reveals Phytoplankton Dynamics, Journal of Environ-
        mental Monitoring, 6, 946–952, https://doi.org/10.1039/B409350J, 2004.

475 Dugenne, M., Thyssen, M., Nerini, D., and Grégori, G. J.: Consequence of a Sudden Wind Event on the Dynamics of a Coastal Phytoplankton
        Community: An Insight into Specific Population Growth Rates Using a Single Cell High Frequency Approach, Frontiers in Microbiology,
        5, https://doi.org/10.3389/fmicb.2014.00485, 2014.

Falkowski, P. G., Barber, R. T., and Smetacek, V.: Biogeochemical Controls and Feedbacks on Ocean Primary Production, Science, 281,
        200–206, https://doi.org/10.1126/science.281.5374.200, 1998.

480 Falkowski, P. G., Laws, E. A., Barber, R. T., and Murray, J. W.: Phytoplankton and Their Role in Primary, New, and Export Production,
        in: Ocean Biogeochemistry: The Role of the Ocean Carbon Cycle in Global Change, edited by Fasham, M. J. R., Global Change — The
        IGBP Series (Closed), pp. 99–121, Springer, Berlin, Heidelberg, ISBN 978-3-642-55844-3, 2003.

Field, C. B., Behrenfeld, M. J., Randerson, J. T., and Falkowski, P.: Primary Production of the Biosphere: Integrating Terrestrial and Oceanic
        Components, Science, 281, 237–240, https://doi.org/10.1126/science.281.5374.237, 1998.

485 Flandrin, P. and Gonçalvès, P.: Empirical Mode Decompositions as Data-Driven Wavelet-like Expansions, International Journal of Wavelets,
        Multiresolution and Information Processing, 02, 477–496, https://doi.org/10.1142/S0219691304000561, 2004.

Flandrin, P., Rilling, G., and Goncalves, P.: Empirical Mode Decomposition as a Filter Bank, IEEE Signal Processing Letters, 11, 112–114,
        https://doi.org/10.1109/LSP.2003.821662, 2004.

Fontana, S. and Pomati, F.: Opportunities and Challenges in Deriving Phytoplankton Diversity Measures from Individual Trait-Based Data
490   Obtained by Scanning Flow-Cytometry, Frontiers in Microbiology, 5, https://doi.org/10.3389/fmicb.2014.00324, 2014.

Fragoso, G. M., Poulton, A. J., Pratt, N. J., Johnsen, G., and Purdie, D. A.: Trait-Based Analysis of Subpolar North Atlantic Phy-
        toplankton and Plastidic Ciliate Communities Using Automated Flow Cytometer, Limnology and Oceanography, 64, 1763–1778,
        https://doi.org/10.1002/lno.11189, 2019.

Fuchs, R., Thyssen, M., Creach, V., Dugenne, M., Izard, L., Latimier, M., Louchart, A., Marrec, P., Rijkeboer, M., Grégori, G., and Pommeret,
495   D.: Automatic Recognition of Flow Cytometric Phytoplankton Functional Groups Using Convolutional Neural Networks, Limnology and
        Oceanography: Methods, 20, 387–399, https://doi.org/10.1002/lom3.10493, 2022.

Genitsaris, S., Monchy, S., Viscogliosi, E., Sime-Ngando, T., Ferreira, S., and Christaki, U.: Seasonal Variations of Marine Protist Community Structure Based on Taxon-Specific Traits Using the Eastern English Channel as a Model Coastal System, FEMS Microbiology Ecology, 91, fiv034, https://doi.org/10.1093/femsec/fiv034, 2015.

500 Gentilhomme, V. and Lizon, F.: Seasonal Cycle of Nitrogen and Phytoplankton Biomass in a Well-Mixed Coastal System (Eastern English Channel), Hydrobiologia, 361, 191–199, https://doi.org/10.1023/A:1003134617808, 1997.

Grattepanche, J. D., Vincent, D., Breton, E., and Christaki, U.: Microzooplankton Herbivory during the Diatom–*Phaeocystis* Spring Succession in the Eastern English Channel, Journal of Experimental Marine Biology and Ecology, 404, 87–97, https://doi.org/10.1016/j.jembe.2011.04.004, 2011.

505 Guiselin, N.: Etude de La Dynamique Des Communautés Phytoplanctoniques Par Microscopie et Cytométrie En Flux, En Eaux Côtière de La Manche Orientale, Ph.D. thesis, Université du Littoral Côte d'Opale, France, 2010.

Halawi Ghosn, R., Poisson-Caillault, É., Charria, G., Bonnat, A., Repecaud, M., Facq, J.-V., Quéméner, L., Duquesne, V., Blondel, C., and Lefebvre, A.: MAREL Carnot Data and Metadata from the Coriolis Data Center, Earth System Science Data, 15, 4205–4218, https://doi.org/10.5194/essd-15-4205-2023, 2023.

510 Hernández-Fariñas, T., Soudant, D., Barillé, L., Belin, C., Lefebvre, A., and Bacher, C.: Temporal Changes in the Phytoplankton Community along the French Coast of the Eastern English Channel and the Southern Bight of the North Sea, ICES Journal of Marine Science, 71, 821–833, https://doi.org/10.1093/icesjms/fst192, 2014.

Hill, M. O.: Diversity and Evenness: A Unifying Notation and Its Consequences, Ecology, 54, 427–432, https://doi.org/10.2307/1934352, 1973.

515 Hobday, A. J., Alexander, L. V., Perkins, S. E., Smale, D. A., Straub, S. C., Oliver, E. C. J., Benthuysen, J. A., Burrows, M. T., Donat, M. G., Feng, M., Holbrook, N. J., Moore, P. J., Scannell, H. A., Sen Gupta, A., and Wernberg, T.: A Hierarchical Approach to Defining Marine Heatwaves, Progress in Oceanography, 141, 227–238, https://doi.org/10.1016/j.pocean.2015.12.014, 2016.

Holland, M., Louchart, A., Artigas, L. F., and Mcquatters-Gollop, A.: Changes in Phytoplankton and Zooplankton Communities Common Indicator Assessment Changes in Phytoplankton and Zooplankton Communities, in: OSPAR, 2023: The 2023 Quality Status Report for

520 the Northeast Atlantic., p. 39, OSPAR Commission, https://hal.science/hal-04404131, 2023.

Houliez, E., Schmitt, F. G., Breton, E., Skouroliakou, D.-I., and Christaki, U.: On the Conditions Promoting *Pseudo-nitzschia* Spp. Blooms in the Eastern English Channel and Southern North Sea, Harmful Algae, 125, 102 424, https://doi.org/10.1016/j.hal.2023.102424, 2023.

Huang, N. E., Shen, Z., Long, S. R., Wu, M. C., Shih, H. H., Zheng, Q., Yen, N.-C., Tung, C. C., and Liu, H. H.: The Empirical Mode Decomposition and the Hilbert Spectrum for Nonlinear and Non-Stationary Time Series Analysis, Proceedings of the Royal Society of

525 London. Series A: Mathematical, Physical and Engineering Sciences, 454, 903–995, https://doi.org/10.1098/rspa.1998.0193, 1998.

Huang, Y., Schmitt, F. G., Lu, Zhiming., and Liu, Y.: Analysis of Daily River Flow Fluctuations Using Empirical Mode Decomposition and Arbitrary Order Hilbert Spectral Analysis, Journal of Hydrology, 373, 103–111, https://doi.org/10.1016/j.jhydrol.2009.04.015, 2009.

Huang, Y. X., Schmitt, F. G., Lu, Z. M., and Liu, Y. L.: An Amplitude-Frequency Study of Turbulent Scaling Intermittency Using Empirical Mode Decomposition and Hilbert Spectral Analysis, Europhysics Letters, 84, 40 010, https://doi.org/10.1209/0295-5075/84/40010, 2008.

530 Hubert, Z., Louchart, A., Robache, K., Epinoux, A., Gallot, C., Cornille, V., Crouvoisier, M., Monchy, S., and Artigas, L. F.: Decadal Changes in Phytoplankton Functional Composition in the Eastern English Channel: Evidence of Upcoming Major Effects of Climate Change?, https://doi.org/10.5194/egusphere-2024-1933, 2024.

Hunter-Cevera, K. R., Neubert, M. G., Olson, R. J., Shalapyonok, A., Solow, A. R., and Sosik, H. M.: Seasons of *Syn*, Limnology and Oceanography, 65, 1085–1102, https://doi.org/10.1002/lno.11374, 2020.

535   Hynes, A. M., Winter, J., Berthiaume, C. T., Shimabukuro, E., Cain, K., White, A., Armbrust, E. V., and Ribalet, F.: High-Frequency
       Sampling Captures Variability in Phytoplankton Population-Specific Periodicity, Growth, and Productivity, Limnology and Oceanography,
       n/a, https://doi.org/10.1002/lno.12683, 2024.

       Jouanneau, N., Sentchev, A., and Dumas, F.: Numerical Modelling of Circulation and Dispersion Processes in Boulogne-sur-Mer
       Harbour (Eastern English Channel): Sensitivity to Physical Forcing and Harbour Design, Ocean Dynamics, 63, 1321–1340,
540   https://doi.org/10.1007/s10236-013-0659-4, 2013.

       Karasiewicz, S., Breton, E., Lefebvre, A., Hernández Fariñas, T., and Lefebvre, S.: Realized Niche Analysis of Phytoplankton Communities
       Involving HAB: *Phaeocystis* Spp. as a Case Study, Harmful Algae, 72, 1–13, https://doi.org/10.1016/j.hal.2017.12.005, 2018.

       Kbaier Ben Ismail, D., Lazure, P., and Puillat, I.: Statistical Properties and Time-Frequency Analysis of Temperature, Salinity and Turbidity
       Measured by the MAREL Carnot Station in the Coastal Waters of Boulogne-sur-Mer (France), Journal of Marine Systems, 162, 137–153,
545   https://doi.org/10.1016/j.jmarsys.2016.03.010, 2016.

       Kim, D. and Oh, H.-S.: EMD: A Package for Empirical Mode Decomposition and Hilbert Spectrum, The R Journal, 1, 40–46,
       https://doi.org/10.32614/RJ-2009-002, 2009.

       Lancelot, C., Thieu, V., Polard, A., Garnier, J., Billen, G., Hecq, W., and Gypens, N.: Cost Assessment and Ecological Effectiveness of
       Nutrient Reduction Options for Mitigating *Phaeocystis* Colony Blooms in the Southern North Sea: An Integrated Modeling Approach,
550   Science of The Total Environment, 409, 2179–2191, https://doi.org/10.1016/j.scitotenv.2011.02.023, 2011.

       Lazure, P. and Desmare, S.: Courantologie. Sous-région Marine Manche - Mer Du Nord. Evaluation Initiale DCSMM., 2012.

       Le Quéré, C., Harrison, S. P., Colin Prentice, I., Buitenhuis, E. T., Aumont, O., Bopp, L., Claustre, H., Cotrim Da Cunha, L., Geider, R.,
       Giraud, X., Klaas, C., Kohfeld, K. E., Legendre, L., Manizza, M., Platt, T., Rivkin, R. B., Sathyendranath, S., Uitz, J., Watson, A. J., and
       Wolf-Gladrow, D.: Ecosystem Dynamics Based on Plankton Functional Types for Global Ocean Biogeochemistry Models, Global Change
555   Biology, 11, 2016–2040, https://doi.org/10.1111/j.1365-2486.2005.1004.x, 2005.

       Lefebvre, A. and Dezécache, C.: Trajectories of Changes in Phytoplankton Biomass, *Phaeocystis Globosa* and Diatom (Incl. *Pseudo-
       nitzschia Sp.*) Abundances Related to Nutrient Pressures in the Eastern English Channel, Southern North Sea, Journal of Marine Science
       and Engineering, 8, 401, https://doi.org/10.3390/jmse8060401, 2020.

       Lefebvre, A., Guiselin, N., Barbet, F., and Artigas, F. L.: Long-Term Hydrological and Phytoplankton Monitoring (1992–2007) of Three
560   Potentially Eutrophic Systems in the Eastern English Channel and the Southern Bight of the North Sea, ICES Journal of Marine Science,
       68, 2029–2043, https://doi.org/10.1093/icesjms/fsr149, 2011.

       Lefebvre, A., Blondel, C., Duquesne, V., Hebert, P., Cordier, R., Belin, C., Huguet, A., Durand, G., Soudant, D., and Devreker, D.: SRN
       Dataset - Regional Observation and Monitoring Program for Phytoplankton and Hydrology in the Eastern English Channel [data set],
       https://doi.org/10.17882/50832, 2024.

565   Legendre, L. and Rassoulzadegan, F.: Plankton and Nutrient Dynamics in Marine Waters, Ophelia, 41, 153–172,
       https://doi.org/10.1080/00785236.1995.10422042, 1995.

       Levoy, F., Anthony, E. J., Monfort, O., and Larsonneur, C.: The Morphodynamics of Megatidal Beaches in Normandy, France, Marine
       Geology, 171, 39–59, https://doi.org/10.1016/S0025-3227(00)00110-9, 2000.

       Lheureux, A., David, V., Del Amo, Y., Soudant, D., Auby, I., Bozec, Y., Conan, P., Ganthy, F., Grégori, G., Lefebvre, A., Leynart, A.,
570   Rimmelin-Maury, P., Souchu, P., Vantrepote, V., Blondel, C., Cariou, T., Crispi, O., Cordier, M.-A., Crouvoisier, M., Duquesne, V.,
       Ferreira, S., Garcia, N., Gouriou, L., Grosteffan, E., Le Merrer, Y., Meteigner, C., Retho, M., Tournaire, M.-P., and Savoye, N.: Trajectories

of Nutrients Concentrations and Ratios in the French Coastal Ecosystems: 20 Years of Changes in Relation with Large-Scale and Local Drivers, Science of The Total Environment, 857, 159 619, https://doi.org/10.1016/j.scitotenv.2022.159619, 2023.

Li, W. K. W.: Cytometric Diversity in Marine Ultraphytoplankton, Limnology and Oceanography, 42, 874–880, https://doi.org/10.4319/lo.1997.42.5.0874, 1997.

Li, W. K. W.: Annual Average Abundance of Heterotrophic Bacteria and *Synechococcus* in Surface Ocean Waters, Limnology and Oceanography, 43, 1746–1753, https://doi.org/10.4319/lo.1998.43.7.1746, 1998.

Li, W. K. W.: Macroecological Patterns of Phytoplankton in the Northwestern North Atlantic Ocean, Nature, 419, 154–157, https://doi.org/10.1038/nature00994, 2002.

Litchman, E., Klausmeier, C. A., Schofield, O. M., and Falkowski, P. G.: The Role of Functional Traits and Trade-Offs in Structuring Phytoplankton Communities: Scaling from Cellular to Ecosystem Level, Ecology Letters, 10, 1170–1181, https://doi.org/10.1111/j.1461-0248.2007.01117.x, 2007.

Lomb, N. R.: Least-Squares Frequency Analysis of Unequally Spaced Data, Astrophysics and Space Science, 39, 447–462, https://doi.org/10.1007/BF00648343, 1976.

Louchart, A., Lizon, F., Lefebvre, A., Didry, M., Schmitt, F. G., and Artigas, L. F.: Phytoplankton Distribution from Western to Central English Channel, Revealed by Automated Flow Cytometry during the Summer-Fall Transition, Continental Shelf Research, 195, 104 056, https://doi.org/10.1016/j.csr.2020.104056, 2020.

Louchart, A., Holland, M., Mcquatters-Gollop, A., and Artigas, L. F.: Changes in Phytoplankton Biomass and Zooplankton Abundance Common Indicator Assessment Changes in Phytoplankton Biomass and Zooplankton Abundance, in: OSPAR, 2023: The 2023 Quality Status Report for the Northeast Atlantic., p. 34, OSPAR Commission, https://hal.science/hal-04404153, 2023.

Louchart, A., Lizon, F., Debusschere, E., Mortelmans, J., Rijkeboer, M., Crouvoisier, M., Lebourg, E., Deneudt, K., Schmitt, F. G., and Artigas, L. F.: The Importance of Niches in Defining Phytoplankton Functional Beta Diversity during a Spring Bloom, Marine Biology: International Journal on Life in Oceans and Coastal Waters, https://doi.org/10.1007/s00227-023-04346-6, 2024.

MAREL Carnot: High Frequency Measurement of the Coastal Environment in the Eastern English Channel. Data from MAREL CARNOT - COAST-HF (Coastal Ocean Observing System - High Frequency) Monitoring Programme within the Research Infrastructure ILICO [data set], https://doi.org/10.17882/39754, 2024.

Menge, D. N. L. and Weitz, J. S.: Dangerous Nutrients: Evolution of Phytoplankton Resource Uptake Subject to Virus Attack, Journal of Theoretical Biology, 257, 104–115, https://doi.org/10.1016/j.jtbi.2008.10.032, 2009.

Olson, R. J., Shalapyonok, A., and Sosik, H. M.: An Automated Submersible Flow Cytometer for Analyzing Pico- and Nanophytoplankton: FlowCytobot, Deep Sea Research Part I: Oceanographic Research Papers, 50, 301–315, https://doi.org/10.1016/S0967-0637(03)00003-7, 2003.

Pal, R. and Choudhury, A. K.: An Introduction to Phytoplanktons: Diversity and Ecology, Springer India, New Delhi, ISBN 978-81-322-1837-1 978-81-322-1838-8, https://doi.org/10.1007/978-81-322-1838-8, 2014.

Peperzak, L., Duin, R., Colijn, F., and Gieskes, W.: Growth and Mortality of Flagellates and Non-Flagellate Cells of *Phaeocystis Globosa* (*Prymnesiophyceae*), Journal of Plankton Research, 22, 107–120, https://doi.org/10.1093/plankt/22.1.107, 2000.

Pomati, F., Kraft, N. J. B., Posch, T., Eugster, B., Jokela, J., and Ibelings, B. W.: Individual Cell Based Traits Obtained by Scanning Flow-Cytometry Show Selection by Biotic and Abiotic Environmental Factors during a Phytoplankton Spring Bloom, PLOS ONE, 8, e71 677, https://doi.org/10.1371/journal.pone.0071677, 2013.

Rantajärvi, E., Olsonen, R., Hällfors, S., Leppänen, J.-M., and Raateoja, M.: Effect of Sampling Frequency on Detection of Natural Variability in Phytoplankton: Unattended High-Frequency Measurements on Board Ferries in the Baltic Sea, ICES Journal of Marine Science, 55, 697–704, https://doi.org/10.1006/jmsc.1998.0384, 1998.

Robache, K., Hubert, Z., Gallot, C., Epinoux, A., Louchart, A. P., Facq, J.-V., Lefebvre, A., Répécaud, M., Cornille, V., Verhaeghe, F., Audinet, Y., Brutier, L., Schmitt, F. G., and Artigas, L. F.: High-Frequency Monitoring of Phytoplankton Functional Groups Using an Automated Flow Cytometer during Two Deployments (2021, 2022) at the MAREL CARNOT Station (Boulogne-sur-Mer, France) in the Eastern English Channel [data set], https://doi.org/10.17882/104948, 2025.

Röthig, T., Trevathan-Tackett, S. M., Voolstra, C. R., Ross, C., Chaffron, S., Durack, P. J., Warmuth, L. M., and Sweet, M.: Human-Induced Salinity Changes Impact Marine Organisms and Ecosystems, Global Change Biology, 29, 4731–4749, https://doi.org/10.1111/gcb.16859, 2023.

Rousseau, V., Vaulot, D., Casotti, R., Cariou, V., Lenz, J., Gunkel, J., and Baumann, M.: The Life Cycle of *Phaeocystis* (*Prymnesiophycaea*): Evidence and Hypotheses, Journal of Marine Systems, 5, 23–39, https://doi.org/10.1016/0924-7963(94)90014-0, 1994.

Ruf, T.: The Lomb-Scargle Periodogram in Biological Rhythm Research: Analysis of Incomplete and Unequally Spaced Time-Series, Biological Rhythm Research, 30, 178–201, https://doi.org/10.1076/brhm.30.2.178.1422, 1999.

Rutten, T. P. A., Sandee, B., and Hofman, A. R. T.: Phytoplankton Monitoring by High Performance Flow Cytometry: A Successful Approach?, Cytometry Part A, 64A, 16–26, https://doi.org/10.1002/cyto.a.20106, 2005.

Sazhin, A. F., Artigas, L. F., Nejstgaard, J. C., and Frischer, M. E.: The Colonization of Two *Phaeocystis* Species (*Prymnesiophyceae*) by Pennate Diatoms and Other Protists: A Significant Contribution to Colony Biomass, in: Phaeocystis, Major Link in the Biogeochemical Cycling of Climate-Relevant Elements, edited by van Leeuwe, M. A., Stefels, J., Belviso, S., Lancelot, C., Verity, P. G., and Gieskes, W. W. C., pp. 137–145, Springer Netherlands, Dordrecht, ISBN 978-1-4020-6214-8, 2007.

Scargle, J. D.: Studies in Astronomical Time Series Analysis. II - Statistical Aspects of Spectral Analysis of Unevenly Spaced Data, Astrophysical Journal, https://doi.org/10.1086/160554, 1982.

Schmitt, F. G., Anneville, O., and Souissi, S.: Dynamique Intermittente Du Plancton : Analyse de La Dynamique Multi-Échelle En Utilisant La Décomposition Modale Empirique, in: Comptes-Rendus de La 16e Rencontre Du Non-Linéaire, pp. 149–154, E Falcon et al Paris, 2013.

Sentchev, A. and Yaremchuk, M.: Monitoring Tidal Currents with a Towed ADCP System, Ocean Dynamics, 66, 119–132, https://doi.org/10.1007/s10236-015-0913-z, 2016.

Serre-Fredj, L., Jacqueline, F., Navon, M., Izabel, G., Chasselin, L., Jolly, O., Repecaud, M., and Claquin, P.: Coupling High Frequency Monitoring and Bioassay Experiments to Investigate a Harmful Algal Bloom in the Bay of Seine (French-English Channel), Marine Pollution Bulletin, 168, 112 387, https://doi.org/10.1016/j.marpolbul.2021.112387, 2021.

Seuront, L.: Hydrodynamic and Tidal Controls of Small-Scale Phytoplankton Patchiness, Marine Ecology Progress Series, 302, 93–101, https://doi.org/10.3354/meps302093, 2005.

Seuront, L., Schmitt, F., Lagadeuc, Y., Schertzer, D., Lovejoy, S., and Frontier, S.: Multifractal Analysis of Phytoplankton Biomass and Temperature in the Ocean, Geophysical Research Letters, 23, 3591–3594, https://doi.org/10.1029/96GL03473, 1996.

Shannon, C. E.: A Mathematical Theory of Communication, Bell System Technical Journal, 27, 379–423, https://doi.org/10.1002/j.1538-7305.1948.tb01338.x, 1948.

SHOM: MNT Topo-Bathymétrique Côtier Du Port de Boulogne-sur-Mer et de Ses Abords à 10m (Projet TANDEM) [data set], https://doi.org/10.17183/MNT_COTIER_PORT_BSM_TANDEM_10m_WGS84, 2015.

SHOM: REFMAR [data set], https://doi.org/10.17183/REFMAR, 2024.

Smith, W. O. and Lancelot, C.: Bottom-up versus Top-down Control in Phytoplankton of the Southern Ocean, Antarctic Science, 16, 531–539, https://doi.org/10.1017/S0954102004002305, 2004.

650 Sosik, H. M., Olson, R. J., Neubert, M. G., Shalapyonok, A., and Solow, A. R.: Growth Rates of Coastal Phytoplankton from Time-Series Measurements with a Submersible Flow Cytometer, Limnology and Oceanography, 48, 1756–1765, https://doi.org/10.4319/lo.2003.48.5.1756, 2003.

Sosik, H. M., Olson, R. J., and Armbrust, E. V.: Flow Cytometry in Phytoplankton Research, in: Chlorophyll a Fluorescence in Aquatic Sciences: Methods and Applications, edited by Suggett, D. J., Prášil, O., and Borowitzka, M. A., Developments in Applied Phycology,

655 pp. 171–185, Springer Netherlands, Dordrecht, ISBN 978-90-481-9268-7, 2010.

Sun, X. and Wang, W.: The Impact of Environmental Parameters on Phytoplankton Functional Groups in Northeastern China, Ecological Engineering, 164, 106 209, https://doi.org/10.1016/j.ecoleng.2021.106209, 2021.

Thyssen, M., Grégori, G. J., Grisoni, J.-M., Pedrotti, M. L., Mousseau, L., Artigas, L. F., Marro, S., Garcia, N., Passafiume, O., and Denis, M. J.: Onset of the Spring Bloom in the Northwestern Mediterranean Sea: Influence of Environmental Pulse Events on the *in Situ* Hourly-

660 Scale Dynamics of the Phytoplankton Community Structure, Frontiers in Microbiology, 5, https://doi.org/10.3389/fmicb.2014.00387, 2014.

Thyssen, M., Grégori, G., Créach, V., Lahbib, S., Dugenne, M., Aardema, H. M., Artigas, L.-F., Huang, B., Barani, A., Beaugeard, L., Bellaaj-Zouari, A., Beran, A., Casotti, R., Del Amo, Y., Denis, M., Dubelaar, G. B. J., Endres, S., Haraguchi, L., Karlson, B., Lambert, C., Louchart, A., Marie, D., Moncoiffé, G., Pecqueur, D., Ribalet, F., Rijkeboer, M., Silovic, T., Silva, R., Marro, S., Sosik, H. M., Sourisseau,

665 M., Tarran, G., Van Oostende, N., Zhao, L., and Zheng, S.: Interoperable Vocabulary for Marine Microbial Flow Cytometry, Frontiers in Marine Science, 9, https://doi.org/10.3389/fmars.2022.975877, 2022.

Tinker, J., Palmer, M. D., Harrison, B. J., O'Dea, E., Sexton, D. M. H., Yamazaki, K., and Rostron, J. W.: Twenty-First Century Marine Climate Projections for the NW European Shelf Seas Based on a Perturbed Parameter Ensemble, Ocean Science, 20, 835–885, https://doi.org/10.5194/os-20-835-2024, 2024.

670 Wickham, H., Averick, M., Bryan, J., Chang, W., McGowan, L. D., François, R., Grolemund, G., Hayes, A., Henry, L., Hester, J., Kuhn, M., Pedersen, T. L., Miller, E., Bache, S. M., Müller, K., Ooms, J., Robinson, D., Seidel, D. P., Spinu, V., Takahashi, K., Vaughan, D., Wilke, C., Woo, K., and Yutani, H.: Welcome to the Tidyverse, Journal of Open Source Software, 4, 1686, https://doi.org/10.21105/joss.01686, 2019.

Wyatt, T.: Margalef's Mandala and Phytoplankton Bloom Strategies, Deep Sea Research Part II: Topical Studies in Oceanography, 101,

675 32–49, https://doi.org/10.1016/j.dsr2.2012.12.006, 2014.

Xiu-ren, N. and Vaulot, D.: Simultaneous Estimates of *Synechococcus* Spp. Growth and Grazing Mortality Rates in the English Channel, Chinese Journal of Oceanology and Limnology, 14, 8–16, https://doi.org/10.1007/BF02850534, 1996.